835

INDC (SWD) 9/G+P

THE SWEDISH RESEARCH COUNCILS' LABORATORY
Studsvik, Fack
S-611 01 Nyköping 1
Sweden

Research report
LF-70
1976
(revised)

CHARACTERIZATION OF DELAYED-NEUTRON SPECTRA

G Rudstam
The Swedish Research Councils' Laboratory
Studsvik, Fack, S-611 01 Nyköping, Sweden

CHARACTERIZATION OF DELAYED-NEUTRON SPECTRA

by

G Rudstam

The Swedish Research Councils' Laboratory,

Studsvik, Fack, S-611 01 Nyköping, Sweden

Abstract

The experimental delayed-neutron spectra of 25 precursors in fission have been described in terms of a series of fine structure peaks superimposed on a gross structure consisting of 1 - 4 components corresponding to different wave-numbers. These precursors are responsible for 85 - 87 % of the delayed-neutron effect in nuclear fuel. By including also some precursors whose spectra have been deduced by an extrapolation procedure the effective delayed-neutron energy distribution in nuclear fuel can be accurately calculated.

As a byproduct the applicability of some recent mass formulas in the region of very neutron-rich nuclei has been tested. Systematic deviations have been found, which indicate the need of further investigations.

1. INTRODUCTION

Recently a large number of delayed-neutron spectra from individual fission products have been measured[1-5]. These spectra can be characterized in terms of a gross structure caused by the interplay of neutron and gamma widths and beta decay properties. Superimposed on this structure, a fine structure may be found which is attributed to the decay of individual nuclear levels, or groups of levels, fed by the preceding beta decay. The latter effect is very pronounced for neutron emitters possessing one neutron above a closed shell,

because of insufficient knowledge of the shape of the response function and its energy dependence. In the present work the intensity of a peak of width a few tens of keV is obtained by summing the contributions from this energy range. This may in certain cases correspond to a single level, but more often the intensity given will be the sum of contributions from two or more closely-spaced levels.

3. THE GROSS STRUCTURE

The gross structure remaining after removing the fine structure as indicated above is treated in the following way. According to Eq. (6) of ref.[2] the neutron spectrum can be expressed as

$$P(E_n)dE_n = \text{const} \sum_J \sum_\ell \frac{\Gamma_n^\ell(E_n)}{\Gamma_n^\ell(E_n) + \Gamma_\gamma} |M_{J\pi}|^2 \rho_{J\pi}(E) f(Z+1, Q_\beta - E) dE_n \qquad (1)$$

where Γ_n^ℓ is the width for the emission of neutrons of wave number ℓ, Γ_γ is the gamma width, $\rho_{J\pi}$ is the density of levels of spin $\underline{J}$ and parity π, $f(Z+1, Q_\beta-E)$ is the Fermi function and $|M|^2$ is the average of the square of the nuclear matrix elements governing the beta decay. The excitation energy of the levels fed by beta decay is denoted by $\underline{E}$ and the neutron energy by E_n. Finally, the total beta decay energy of the precursor is denoted by Q_β and the neutron separation energy of the emitter by B_n. Apparently, neglecting the kinetic energy of the recoiling nucleus, one finds

$$E_n \leq E - B_n \qquad (2)$$

with the equality sign valid for neutron decay to the ground state of the final nucleus (the case of gamma emission preceding the neutron emission is neglected).

Eq. (1) can be simplified in various ways. Beta strength studies have shown that the matrix element factor can be regarded as energy-independent[8]. For the shape of the various terms in Eq. (1) only the energy-dependent part of the factors need be considered. Thus, the spin part of the level density function can be taken out leaving

$$\rho(E) = \text{const} \times \exp\,(2(aU)^{1/2})/U^{5/4}, \qquad (3)$$

with $U = E - P$, where P is the total pairing energy (can be taken from ref.[9]). The level density parameter a is also obtained from ref.[9]. The Fermi function is approximated by the expression[10)]

$$f(Z+1,\ Q_\beta - E) = \text{const} \times (Q_\beta - E)^5. \qquad (4)$$

The neutron width $\Gamma_n^{(\ell)}$ is proportional to the neutron transmission constant T_ℓ which can be determined from the optical model. In the present work a modified form of the ABACUS programme[11,12)] has been used. The neutron branching ratio S_ℓ can then be written (assuming only one predominant neutron wave).

$$S_\ell = \frac{\Gamma_n^{(\ell)}}{\Gamma_n^{(\ell)} + \Gamma_\gamma} = \frac{T_\ell}{T_\ell + k\Gamma_\gamma}. \qquad (5)$$

It now remains to determine the term $k\Gamma_\gamma$ which should vary so slowly with energy that it can be considered as energy-independent. The term can be determined by noting the position of the maximum of a neutron distribution $P_\ell(E)dE$ attributed to a particular wave number. This distribution can be written

$$P_\ell(E_n)dE_n = C_\ell S_\ell(E_n)\ \frac{e^{2\sqrt{a(E-P)}}}{(E-P)^{5/4}}(Q_\beta - E)^5\, dE_n, \qquad (6)$$

with C_ℓ being a normalization constant.

For a case with all neutrons feeding the ground state of the final nucleus, i.e. with $E = B_n + E_n$, the P_ℓ-function will have a maximum at a neutron energy satisfying the equation

$$\frac{dS_\ell(E_n)}{dE_n} + S_\ell(E_n)\Big\{(a/(B_n + E_n - P))^{1/2} - \frac{5}{4}(B_n + E_n - P)^{-1} -$$

$$- 5(Q_\beta - B_n - E_n)^{-1}\Big\} = 0. \qquad (7)$$

Furthermore, from Eq. (5):

$$\frac{dS_\ell}{dE_n} = \frac{\frac{dT_\ell}{dE_n} \times k\Gamma_\gamma}{(T_\ell + k\Gamma_\gamma)^2}. \qquad (8)$$

By examining the experimental P_ℓ-distribution the neutron energy E_m corresponding to its maximum can be found. It is then used for calculating the value $Z(E_m)$ of the expression within the curly brackets of Eq. (7). Then

$$k\Gamma_\gamma = - \frac{Z(E_m)\left[T_\ell(E_m)\right]^2}{Z(E_m)\,T_\ell\,(E_m) + \left[dT_\ell/dE_n\right]_{E_m}} . \tag{9}$$

By introducing calculated values, at the energy E_m, of the transmission coefficient and its derivative into Eq. (9) a determination of the term $k\Gamma_\gamma$ results. Finally, the value of the normalization constant C_ℓ of the contribution P_ℓ can be obtained by equating the integrated experimental distribution corresponding to the wave number ℓ and the integral of Eq. (6).

If the neutrons do not feed the ground state of the final nucleus, the shape of the neutron spectrum will be modified. For a given neutron energy the level density factor will increase but this effect is counteracted by a decrease of the Fermi function. In addition, the spectrum will be shortened and only reach the energy $Q_\beta - B_n - E_\gamma$ where E_γ is the energy of the level fed. The contribution is still described by Eq. (6) with the excitation energy E now set equal to $B_n + E_n + E_\gamma$. A further modification will have to be introduced if several levels can be reached by the emission of neutrons of the same wave number. Then the denominator of the neutron branching ratio should contain all the $\Gamma_n^{(\ell)}$-values (T_ℓ-values) concerned.

It should normally be sufficient to take only contributions of wave numbers corresponding to the de-excitation of levels fed by allowed beta-decay into account. Only if this does not adequately represent the gross structure in the measured spectra, contributions from levels fed by forbidden beta-decay may also be included.

4. EXAMPLE: ^{137}I

The precursor ^{137}I feeds, by allowed beta decay, $5/2^+$-states in ^{137}Xe, which emit d-wave neutrons to the ground state of ^{136}Xe. Allowed transitions may also feed $7/2^+$ - and $9/2^+$-levels with the subsequent emission of g-wave neutrons. In addition, the first excited state of ^{136}Xe, at 1.313 MeV, is attainable by s-wave neutron emission. The neutron spectrum should therefore exhibit one P_o, one P_2 and one P_4-term, i.e.

$$P(E_n)dE_n = P_o(E_n)dE_n + P_2(E_n)dE_n + P_4(E_n)dE_n \qquad (10)$$

The experimental spectrum (cf. ref.[2]) contains a number of discrete peaks and then, in addition, a remaining more or less continuous distribution. The envelope of the d-wave neutrons seems to peak around 400 keV. There is no evident g-wave component in the ^{137}I spectrum but the spectrum of ^{135}Sb indicates a g-wave component peaking around 1000 keV[2]. Using these findings and putting $a = 12.99\ \text{MeV}^{-1}$[9], $P = 1.32$ MeV[9], and $B_n = 3.86$ MeV[13] there remain the Q_β-value and the normalization constants of the various gross structure components to be fixed by a comparison with the experimental spectrum. The resulting curve obtained by adding the fine structure peaks (evaluated from the experimental spectrum) to the s-, d-, and g-wave components is shown in Fig. 1. Evidently, the calculated curve (dotted curve) adheres closely to the experimental spectrum (histogram). The parameters used in the calculation are given in Table 1, and the quantities deduced from the fitting procedure are collected in Table 2.

The intensities are normalized to the experimental neutron branching ratio of 5.40 %[14]. To this figure the s-wave continuum contributes 0.52 %, the d-wave continuum 2.23 %, the g-wave continuum 0.65 % and the fine structure peaks 2.00 %.

The transmission coefficients were calculated using optical model parameters from ref.[15]. A set of values used for interpolation is given in Tables 3 and 4 (for ^{137}Xe and ^{87}Kr, respectively). It should be noted that other ways of calculating the transmission coefficients, for instance from the formulas of ref.[16], could also have been used without changing the final results much. The reason for this is that the probability of emitting neutrons is adjusted via the term $k\Gamma_\gamma$.

5. THE DELAYED NEUTRON SPECTRA FROM PRECURSORS APPEARING IN FISSION

The analysis outlined in the preceding chapters has been applied to 25 delayed-neutron spectra. All these except the one for the precursor ^{85}As have been measured in this laboratory. The parameters appearing in the level density formula, i.e. a and P, the total disintegration energy Q_β, the neutron separation energy B_n, and the neutron branching ratio P_n are tabulated in Table 1. The quantities describing the gross structure of the spectra, E_γ, C_ℓ, and $k\Gamma_\gamma$, are collected in Table 2 which also contains the energies and intensities of the fine structure peaks.

It should be noted that the neutron branching ratios have only been used for normalizing the spectra. Some of the P_n-values are known with very little precision. When better values will become available in the future, the C_ℓ-parameters and the peak intensities may be corrected by multiplying them by the new value and dividing them by the old one. There has been no attempt to use the spectra for calculating the P_n-values (c.f. ref.[2]) . It may also be noted that the procedure adopted here is not very sensitive to the relative intensities of the various gross structure components.

As the transmission coefficients vary slowly with nuclear mass, those of Table 3 have been used throughout for the precursors at the heavy mass peak and those of Table 4 for the precursors at the light mass peak. For heavy precursors the gross structure components were assumed to peak at 10 keV, 10 keV, 400 keV, 600 keV,and 1000 keV for ℓ=0,1,2,3 and 4, respectively. For light precursors the values 10 keV, 10 keV, 200 keV, 400 keV, and 700 keV were chosen for ℓ = 0, 1, 2, 3, and 4, respectively (cf. refs.[2] and [28]).

The calculated energy distributions can be compared to the experimental spectra in Figs. 1 - 25. The normalization of the experimental spectra is slightly adjusted to take into account that the experimental spectrum does not extend to zero neutron energy and that, apparently, the high-energy wing of the thermal neutron peak has not been properly subtracted in all cases.

In view of the semi-empirical nature of the present treatment the possible effect on the shape of the gross structure components, arising from competition between them, is neglected.

6. COMPARISON WITH EXPERIMENTAL TOTAL DECAY ENERGIES AND WITH MASS FORMULA PREDICTIONS

It must be borne in mind that the main purpose of the present treatment is to find suitable representations of the delayed-neutron energy spectra. Nevertheless, it is possible to draw some interesting conclusions of a more basic nature from the results; the most important one concerning the values of the total decay energies and neutron separation energies required for an acceptable fit of the calculated distributions to the experimental spectra.

The first task is to find out the precision of the present evaluation. To investigate this calculations have been performed for ^{88}Br (chosen because the neutron spectrum can be described by a single gross structure component) using 7.08 MeV for the neutron separation energy and varying the Q_β-value from 8.4 to 8.7 MeV. The results are shown in Fig. 26. Apparently 8.4 MeV is too low and 8.7 MeV too high. An examination indicates that the value should be between 8.5 and 8.6 MeV to give an acceptable fit. Thus, the precision of the procedure is of the order of 100 keV which is very satisfactory. Obviously, the precision will depend on the statistical accuracy of the experimental points.

Next, it is important to check the validity of the present treatment by comparing the decay energies obtained with experimental determinations. Unfortunately, the experimental data are still scarce. The data available are collected in Table 5. On the whole, the agreement is acceptable. For ^{93}Rb two widely different Q_β-values have been published[32,44]. The result deduced in the present work supports the higher value. There is reason to question the lower one because it corresponds to a maximum neutron energy of 0.64 ± 0.15 MeV which is incompatible with the fact that the experimental neutron spectrum extends to at least 1.25 MeV (cf. Fig. 11). This means that either the experimental Q_β-value is too low or the B_n-value (from ref.[13]) is too high.

The conclusion from the above-mentioned tests is that the indirect method used in the present work leads to Q_β-values with good precision and in fair agreement with direct experimental determinations in the few cases where such data exist. It is therefore suitable for checking various mass formulas. Predictions obtained from the mass formulas by Garvey et al[17)], by Myers and Swiatecki[18)], by Liran and Zeldes[19)], and by Seeger and Howard[20)] have been included in Table 1 for a comparison with the Q_β- and B_n-values deduced from the present approach. As this treatment is sensitive to the neutron window $Q_\beta - B_n$ rather than to the mass data themselves, the comparison should be based on that quantity.

The predicted value of the neutron window, divided by the value determined in the present work, is plotted versus the mass number of the precursor in Fig. 27. All the mass formulas tested give similar results with large deviations from unity for many precursors. Moreover, the diagram reveals a definite trend for isotopic series. This trend is very obvious for bromine and iodine. Five isotopes of these elements have been studied, and in both cases the ratio increases quite regularly with increasing mass. The same trend is noticeable for isotopes of gallium, rubidium, indium, and cesium as well.

One interpretation of the systematic deviation found above is that all the mass formulas fail in the region of very neutron-rich fission products. Before drawing this conclusion there are two further checks to be made, however. It must be kept in mind that the analysis rests on the assumption that the matrix elements governing the beta decay are independent of the excitation energy of the daughter. This assumption is backed up by experimental evidence[8,34)]. In spite of this, a test has been made of the effect caused by replacing the assumption of an energy-independent matrix element by the assumption that the beta strength is independent of energy which is valid for neutron-deficient nuclei[35]. This will in general widen the neutron window because the feeding of lower excitation energies is enhanced, and a higher Q_β-value is required for an acceptable fit to the experimental spectrum. The systematic trends will remain, however, as indicated for iodine isotopes by the dotted curve in Fig. 27.

Another possible explanation is that the feeding of the ground states of the final nuclei is negligible for heavy bromine, rubidium, and iodine isotopes (and also for ^{85}As) whereas this need not be the case for gallium, indium, and cesium precursors, nor for light isotopes of bromine, rubidium, and iodine. Such a behaviour can, in fact, be checked experimentally, and a programme with this aim has started at this laboratory. Until quantitative results have emerged from the study, the question about the validity of the mass formulas of refs.[17-20] far out on the neutron-rich side os stability, important for calculations on nucleosynthesis, must be left open.

The gamma correction term $k\Gamma_\gamma$ is defined by Eq. (5). According to ref.[36] the constant $\underline{k}$ may be written

$$k_{(\ell)} = \frac{2\pi}{D_{(\ell)}} , \qquad (10)$$

where $D_{(\ell)}$ is the spacing of those levels which emit ℓ-wave neutrons. Thus, in principle it should be possible to derive the radiation width from the value of $k\Gamma_\gamma$. However, as this term was used essentially as a free parameter this line is hardly worth pursuing.

7. THE NON-MODERATED DELAYED-NEUTRON ENERGY SPECTRUM IN NUCLEAR FUEL

In the introduction of this article the importance of knowing the virginal energy spectrum of the delayed neutrons emitted in nuclear fuel was stressed. Apparently, this distribution arises by summing the contributions from all precursors appearing in fission, *i.e.* by weighting the individual spectra by the abundances of the various precursors. In order to calculate the abundances one needs to know the original composition of the fuel, the irradiation history, the half-lives, the delayed-neutron branching ratios, and the neutron capture cross sections of all the fission products and actinides. The general evaluation gets quite complicated but, fortunately, the calculation can be simplified because of the position of most of the precursors way out on the neutron-richer side of the peaks of the charge distributions. This means that the parent effect is usually small - the parents have smaller yields than the precursors. In addition, the parents are usually more short-lived than the precursors and rapidly saturated. It is then sufficient to take them into account by using the cumulative yields of the precursors in the following - approximate but quite accurate - formula for the delayed-neutron activity as a function of time *t* after stopping the fission process of length *T*:

$$P(E_n)dE_n = N \sum_j Y_j(1 - e^{-\lambda_j T})e^{-\lambda_j t} P_j(E_n)dE_n, \qquad (11)$$

where *N* is the fission rate during the irradiation, and Y_j and λ_j are the yield (cumulative and properly weighted if the fuel contains several fissionable components) and the decay constant of the precursor *j*. The delayed-neutron energy spectrum, normalized to the P_n-value and corresponding to the precursor *j*, is denoted by $P_j(E_n)dE_n$.

The present work contains descriptions of the spectra of 25 precursors. Taking thermal-neutron fission of ^{235}U as an example and using recommended cumulative yields from ref.[47] and P_n-values from Table 1 and from ref.[14] one finds that these precursors emit 121 delayed neutrons per 10^4 fissions which is 87 % of the delayed neutrons from known precursors (139 neutrons per 10^4 fissions).

Thus, the measured spectra are already quite representative for the total effect. The most important cases not yet included are (number of delayed neutrons per 10^4 fissions within brackets): ^{93}Kr (1.0), ^{96}Rb (2.3), ^{97}Rb (0.7), ^{97}Y (7.9), and ^{99}Y (2.2). An effort should be made to measure the spectra of these cases, but before this is done it is possible to take them into account in the following way. The neutron window of ^{97}Rb is estimated by a linear extrapolation of those of ^{93}Rb and ^{95}Rb, which gives 3.8 MeV. The same gradient is used for the pair ^{94}Rb - ^{96}Rb, which gives a neutron window of about 3.3 MeV for the latter precursor. Using for the neutron binding energy an average of the mass formula predictions in refs.[17-20] this procedure fixes B_n and Q_β. Furthermore, the neutron spectrum of ^{96}Rb may be expected to be similar to that of ^{94}Rb (the same ratio between p-wave and f-wave gross structure components is assumed). In the same way, ^{97}Rb is compared to ^{95}Rb. Thus, the neutron spectra of ^{96}Rb and ^{97}Rb are constructed in analogy with those of the lighter rubidium isotopes.

For the precursor ^{93}Kr no extrapolation procedure is possible. From estimates of its ground state spin ($5/2^+$) and the spin of the final product ^{92}Rb (4^-) it is evident that p- and f-wave neutron emission would be possible. The neutron binding energy is assumed to be 6.11 MeV[13] and for the neutron window an average of the predictions from refs.[17-20] is used. This gives the value 1.61 MeV or closely the same as found for ^{93}Rb in this work. With this as basis the ratio between p- and f-wave neutron emission is assumed to be the same as for ^{93}Rb.

The ground state spins and parities of ^{97}Y and ^{99}Y are tentatively put equal to $1/2^-$. This would allow p-wave and f-wave neutron emission to the ground state of the final product. For ^{99}Y a similar procedure is adopted as for ^{93}Kr. For ^{97}Y, on the other hand, the mass formulas disagree on whether this should be a precursor, and both B_n and Q_β are taken from ref.[13]. The neutron window is low but, lacking more information, the ratio between the p- and f-wave components is taken to be that corresponding to ^{93}Rb.

Including the five cases with estimated neutron spectra, the precursors taken into account will emit more than 97 % of all the delayed neutrons from known precursors. Their combined spectra should therefore correspond very closely to the effective delayed-neutron spectrum in the fission of ^{235}U. Those identified cases, which are neglected here, cannot possibly change the resulting spectrum much.

According to Keepin[37] the experimental number of delayed neutrons in thermal neutron induced fission of ^{235}U is 158±5 per 10^4 fissioning nuclei. This number is higher than the figure 139 for known precursors used here. However, many of the P_n-values are very uncertain and, in addition, recent experimental evidence showing large even-odd effects [38] have cast some doubts on extrapolation procedures such as the one adopted in ref.[47] for the evaluation of fission yields. Therefore, the evaluated number is very uncertain, and it is not possible to state what percentage of the total delayed-neutron activity which corresponds to unknown precursors. It may be mentioned that Amiel[39] arrives at a total of 160±8 dealyed neutrons per 10^4 fissioning nuclei in accordance with the experimental figure by summing the effect of essentially the same precursors as in the present work but with somewhat different yields and P_n-values.

Awaiting more precise experimental data on yields and P_n-values it seems justified to assume that the effect of the precursors, as yet unknown, on the shape of the effective delayed-neutron spectrum cannot be large. Thus the spectrum calculated using Eq. (11) including the known and estimated neutron spectra should be an accurate representation of the non-moderated delayed-neutron spectrum in fission.

If ^{239}Pu is chosen instead of ^{235}U as the fissionable material, the 25 cases treated here correspond to 85 % of the total neutron activity of identified precursors, and this percentage increases to 99 % when the estimated spectra are included. In this case the total effect of known precursors amounts to 62 delayed neutrons per 10^4 fissioning nuclei in agreement with the experimental result 61±3 for an unseparated sample[37].

The use of Eq. (11) now permits the calculation of the effective delayed-neutron energy distribution in nuclear fuel for any irradiation and cooling conditions. An example is given in Fig. 28 containing delayed-neutron spectra for a long irradiation of ^{235}U with thermal neutrons and varying the cooling times. The origin of the main fine structure peaks is indicated. The evolution of the spectra with cooling time is clearly seen.

It should be noted that the experimental data for individual precursors used as basis for describing the spectra do not extend below about 70 keV. Consequently, any possible fine structure below this energy is not reproduced although the general shape should be valid down to very low energies. The lowest energy used in the calculation is 10 keV. At some point below this energy even the s-wave components of the spectra will decrease towards zero as a result of decreasing transmission coefficients. This rapid change of the composite spectrum at low energy is not shown in the figures.

The results obtained in the present work can be compared to integral measurements reported in literature[40-43] where a certain experimental sequence (recycling of the sequence: irradiation of length T, cooling of length t_c, measurement of length t_m, total cycling time t_{tot}) has been followed. By integrating Eq. (11) over the measuring period and summing the contributions from the different cycles (cf. ref.[40]) it is possible to arrive at a neutron distribution which should correspond closely to the measured conditions. Since the number $\underline{n}$ of cycles is not always mentioned in the reports it is assumed here that it is so large that the term $\exp(-n\lambda t_{tot})$ is negligible for all precursor half-lives. The resulting distributions are compared to measured spectra from refs.[41-43] in Figs. 29 - 32.
The experimental conditions are given in the captions.

From the work of Shalev and Cuttler[41] the distribution in the 4-11 "subgroups" of the "long cycle" irradiation of ^{235}U is chosen for a comparison with the results of the present work. Shalev and Cuttler analyze their results in terms of discrete peaks which are indicated as lines in Fig. 29. Apparently, the agreement is excellent. All main peaks found by Shalev and Cuttler have their counterparts as fine structure peaks in the calculated distribution (sometimes displaced about 10 keV which is within the limit of errors).

In order to compare the general shapes of the distributions the Shalev-Cuttler results have been smoothed and normalized to contain the same number of neutrons in the energy range 100 - 1200 keV as the calculated curve. It is seen from Fig. 29 that the smoothed curve, indicated by a broken line, agrees very well with the calculated one.

Next, results for two different time sequences obtained by Fieg[42] are compared to distributions calculated for these experimental conditions in Figs. 30 and 31. The agreement is good although Fieg's "long cycle"-spectrum is possibly somewhat harder than the calculated one.

Finally, the distribution corresponding to the "4-second cycle" of Sloan and Woodruff[43] has been plotted in Fig. 32 together with a calculated distribution. As mentioned above the peaks at energies below about 70 keV cannot be reproduced in the calculated curve. The other peaks found by Sloan and Woodruff have their counterparts in the calculated curve (where they do not stand up so well because they have been spread out over 30 keV) except the one at 215 keV. As for the general shape of the distributions the agreement is poor, however. The neutron spectrum determined by Sloan and Woodruff is considerably softer than the calculated one. Similar results are obtained for the "12-second cycle" and the "25-second cycle" of ref.[43]. This discrepancy stays unexplained.

The spectrum in Fig. 28, for which the cooling time is zero, is of special interest because it corresponds to the equilibrium spectrum of the delayed neutrons in ^{235}U. Several authors have tried to evaluate the equilibrium spectrum from experiments of the kind described above. The results cannot be expected to be very accurate, however, firstly because the evaluations are based on the approximate lumping of the precursors into a number of "half-life groups" and, secondly, because the precursors of half-lives below one second are only very crudely, if at all, taken into account. In spite of these shortcomings the evaluated spectra agree surprisingly well with the equilibrium spectrum obtained in the present work as is seen from Fig. 33 where the equilibrium neutron distribution deduced by Fieg[42] has been chosen for the comparison.

So far, the neutron spectra have been calculated for thermal neutron induced fission of ^{235}U. In a similar way the spectra can be calculated for any fissionable material or mixture of fissionable components. As a further example the equilibrium delayed-neutron spectrum corresponding to thermal neutron induced fission of ^{239}Pu is plotted in Fig. 33. Apparently, its shape is very similar to that for ^{235}U.

8. CONCLUSIONS

The experimental delayed-neutron spectrum of an individual precursor can be accurately characterized by a series of fine structure peaks superimposed on a gross structure consisting of 1 - 4 components corresponding to different wave numbers. Such descriptions have been given for 25 precursors which together are responsible for 87 % of the delayed-neutron effect of known precursors in the thermal-neutron induced fission of ^{235}U. The corresponding figure for ^{239}Pu is 85 %. The spectra of another five precursors have been deduced by an extrapolation procedure bringing the percentage up to 97 for ^{235}U and 99 for ^{239}Pu. By summing all these spectra, using precursor abundances as weights, it is possible to construct the effective non-moderated delayed-neutron spectrum for any irradiation conditions and cooling times. The spectra agree well with experimental determinations.

It has been customary to classify the precursors in a series of "half-life groups". This approach was useful at the time when the knowledge about the individual precursors was very incomplete. This is no longer the case. The old classification, which is inaccurate and completely without any scientific foundation, should therefore be abandoned. Instead, the information recently made available concerning the properties of the delayed-neutron precursors should be used for more accurate evaluations of the delayed-neutron effect at any experimental conditions which happen to be of interest.

The experimental spectra forming the basis of the spectrum descriptions run from about 70 keV up to about 1800 keV. Any fine structure below 70 keV is not recorded. Thus, there is need for improvements in the low-energy end of the spectra. In the region above 70 keV the measured spectra are probably sufficiently good, but those cases for which the spectra have only been obtained by extrapolation need to be measured. This list consists of ^{93}Kr, ^{96}Rb, ^{97}Rb, ^{97}Y, and ^{99}Y. To the list should probably be added ^{98}Y, which might be important. Apart from these improvements in the measurements of spectra there is a great need for improving the knowledge about neutron branching ratios. In this field there are large discrepancies between different determinations and, on the whole, the situation is rather unsatisfactory. Another field requiring better knowledge is the fission yields of the precursors where, so far, very little experimental data exist. The yields are usually determined by extrapolations, a procedure which is possibly subject to large uncertainties.

As a side result of the present treatment the applicability of some recent mass formulas for very neutron-rich nuclei has been tested. Some systematic deviations have been found which indicate that the mass formulas might fail in this region. This is an important result especially with respect to the applicability of the mass formulas for regions still further away from stability, i.e. for studies of nucleosynthesis via the r-process. For more definite conclusions, however, additional information is needed, expecially on the question about the delayed-neutron feeding of excited states of the final nucleus.

Acknowledgements

This work has been supported by the Swedish Council for Atomic Research.

REFERENCES

1) G Rudstam, S Shalev, and O C Jonsson, Nucl. Instr. Methods <u>120</u> (1974) 333.

2) S Shalev and G Rudstam, Nucl. Phys. <u>A230</u> (1974) 153.

3) G Rudstam and S Shalev, Nucl. Phys. <u>A235</u> (1974) 397.

4) S Shalev and G Rudstam, Nucl. Phys. <u>A275</u> (1977) 76.

5) H Franz, J-V Kratz, K-L Kratz, W Rudolph, G Herrmann, F M Nuh, S G Prussin and A A Shihab-Eldin, Phys. Rev. Letters <u>33</u> (1974) 860.

6) J R Huizenga and L G Moretto, Ann. Rev. Nucl. Sci. 22 (1972) 427.

7) S Yiftah and D Saphier, Trans. Am. Nucl. Soc. <u>11</u> (1968) 568.

8) K Aleklett, G Nyman and G Rudstam, Nucl. Phys. <u>A246</u> (1975) 425.

9) J W Truran, A G W Cameron and G Hilf, CERN Report 70-30 (1970) 275.

10) A M Poskanzer, R A Esterlund and R McPherson, Phys. Rev. Lett. <u>15</u> (1965) 1030.

11) E H Auerbach, Brookhaven National Laboratory Report BNL 6562 (1974).

12) G Rudstam, The Swedish Research Councils' Laboratory Report LF-63 (1975).

13) A H Wapstra and N B Gove, Nucl. Data Tables <u>9</u> (1971) 267.

14) L Tomlinson, Atomic Data and Nuclear Data Tables <u>12</u> (1973) 179.

15) C M Perey and F G Perey, Atomic Data and Nuclear Data Tables <u>13</u> (1974) 293.

16) J M Blatt and V F Weisskopf, Theoretical Nuclear Physics, John Wiley & Sons, New York 1952, p. 361.

17) G T Garvey, W J Grace, R L Jaffe, I Talmi and I Kelson, Revs. Mod. Phys. <u>41</u> (1969) S1.

18) W D Myers and W J Swiatecki, Droplet Model Mass Table (1975), (unpublished).

19) S Liran and N Zeldes, Institut für Kernphysik, Technische Hochschule Darmstadt Report IKDA 75/14 (1975), (unpublished).

20) P A Seeger and W M Howard, Nucl. Phys <u>A238</u> (1975) 491 and American Report LA-5750.

21) M Asghar, J P Gautheron, G Bailleul, J P Bocquet, J Greif, H Schrader, G Siegert, C Ristori, J Grançon, and G I Crawford, Nucl.Phys. A247 (1975) 359.

22) H D Schussler, H Ahrens, H Folger, H Franz, W Grimm, G Herrmann, F V Kratz, and K L Kratz, Proc. 2nd Conf. on Physics and Chemistry of Fission, Vienna, 1969 (IAEA, Vienna, 1969)p. 591.

23) K L Kratz and G Herrmann, Nucl. Phys. A229 (1974) 179.

24) M Asghar, J Crançon, J P Gautheron and C Ristori, J.Inorg. Nucl. Chem. 37 (1975) 1563.

25) S Amiel, Proc. 2nd Conf. on Physics and Chemistry of Fission, Vienna, 1969 (IAEA, Vienna, 1969) p. 569.

26) G Rudstam and E Lund, The Swedish Research Councils' Laboratory Report LF-77 (1976).

27) H Franz, J V Katz and G Herrmann, private communication, 1972. See also ref.[5].

28) K Takahashi, Progr. Theor. Phys. 47 (1972) 1500.

29) M I Macias-Marques, R Foucher, M Cailliau, and J Belhassen, CERN Report 70-30 (1970) p. 321.

30) K Aleklett, E Lund, and G Rudstam, The Swedish Research Councils' Laboratory Report LF-71 (1976) and Proceedings of the 3rd International Conference on Nuclei far from Stability, Cargèse, Corsica, 19-26 May, 1976.

31) K Aleklett and E Lund, private communication, 1976.

32) R Brissot, F Schussler, E Monnand and A Moussa, Nucl. Phys. A238 (1975) 149.

33) K Wünsch, H Wollnik, and G Siegert, Phys. Rev. 10C (1974) 2523.

34) K H Johansen, K Bonde Nielsen, and G Rudstam, Nucl. Phys. A203 (1973) 481.

35) C L Duke, P G Hansen, O B Nielsen,and G Rudstam, Nucl. Phys. A151 (1970) 609.

36) Ref.[16] p. 289.

37) G R Keepin, Physics of Nuclear Kinetics, Chapter 4 (Addison-Wesley, 1965).

38) S Amiel and H Feldstein, IAEA/SM-174/25 (1973).

39) S Amiel, Proceedings of a Panel on Fission Product Nuclear Data, Bologna, 26-30 November 1973, Vol 2, p. 33 (IAEA, Vienna, 1974).

40) R Batchelor and H R McK Hyder, J. Nucl. Energy 3 (1956) 7.

41) S Shalev and J M Cuttler, Nucl. Sci. Eng. 51 (1973) 52.

42) G Fieg, J. Nucl. Energy 26 (1972) 585.

43) W R Sloan and G L Woodruff, Nucl. Sci.and Eng. 55 (1974) 28.

44) J R Clifford, W L Talbert, Jr., F K Wohn, J P Adams,and J R McConnell, Phys. Rev. C7 (1973) 2535.

45) A Kerek, G B Holm, S Borg,and P Carlé, Nucl. Phys. A209 (1973) 520.

46) J P Adams, G H Carlson, M A Lee, W L Talbert, Jr., F K Wohn, J R Clifford,and J R McConnell, Phys. Rev. C8 (1973) 767.

47) M E Meek and B F Rider, American Report NEDO-12154-1 (1974).

Table 1

Parameters used in the calculation of the gross structure components

Precursor	a [a)] MeV^{-1}	P [a)] MeV	P_n [b)] %		Q_β / B_n Present work	Wapstra and Gove [c)]	MeV Garvey et al [d)]	Myers and Swiatecki [e)]	Liran and Zeldes [f)]	Seeger and Howard [g)]
^{79}Ga	10.03	1.201	(1)	Q_β	6.76 [m)]		6.06	5.65	6.66	6.26
				B_n	5.15	5.68±0.64	5.70	6.00	5.87	5.87
^{80}Ga	9.70	2.542	(1)	Q_β	8.60 [m)]		9.44	8.74	9.64	9.48
				B_n	7.40		8.50	8.47	7.95	8.36
^{81}Ga	9.25	1.201	(10)	Q_β	7.23 [m)]		7.44	6.97	8.39	7.87
				B_n	5.15		5.13	5.57	5.26	5.60
^{85}As	9.58	1.449	20	Q_β	6.50		9.05	8.25	9.83	8.83
				B_n	4.00		4.10	3.76	4.09	4.54
^{87}Br	9.89	1.331	2.3	Q_β	6.60	6.50(s)	6.68	5.97	6.91	6.43
				B_n	5.511	5.51±0.01	5.46	4.66	5.53	5.49
^{88}Br	10.46	2.152	4.6	Q_β	8.55		8.98	8.93	9.65	9.18
				B_n	7.08	7.08±0.10	7.15	7.05	7.02	7.06
^{89}Br	11.05	1.331	8.6	Q_β	6.80		8.04	7.33	8.58	7.79
				B_n	4.93	4.93±0.11	5.22	4.31	4.74	4.76
^{90}Br	11.61	2.145	12	Q_β	9.00		10.33	10.10	11.31	10.71
				B_n	6.40	6.40±0.11	6.21	6.67	6.39	6.58
^{91}Br	12.18	1.331	8.3	Q_β	6.80		9.18	8.16	10.00	9.17
				B_n	4.69	4.69 (s)	4.57	4.00	4.07	4.12
^{93}Rb	11.95	1.272	1.2 [h)]	Q_β	6.72	6.90 (s)	6.62	5.85	7.11	6.84
				B_n	5.11	5.11±0.10	5.14	4.88	5.12	5.01
^{94}Rb	12.49	2.367	9.6 [h)]	Q_β	10.14 [p)]		9.45	8.57	9.71	9.82
				B_n	7.90	6.86±0.23	7.17	7.51	6.77	6.97
^{95}Rb	13.04	1.272	8.4 [h)]	Q_β	8.59 [p)]		7.87	6.87	8.36	7.64
				B_n	5.90	4.87 (s)	4.64	4.98	4.51	4.31

Table 1 (continued)

Precursor	a [a)] MeV^{-1}	P [b)] MeV	P_n [b)] %		Present work	Wapstra and Gove c)	Garvey et al d)	Myers and Swiatecki e)	Liran and Zeldes f)	Seeger and Howard g)
					Q_β /B_n MeV					
^{129}In	10.93	1.307	(10)	Q_β	7.52 [m)]		7.31	6.80	7.08	7.20
				B_n	5.60		5.32	5.33	5.38	5.23
^{130}In	10.39	2.369	(10)	Q_β	9.30 [q)]		9.69	9.19	9.37	9.69
				B_n	7.40		7.42	7.32	7.34	7.39
^{134}Sn	10.96	0	17 [h)]	Q_β	5.50		6.07	6.06	8.12	6.42
				B_n	3.00		3.43	3.23	2.90	3.42
^{135}Sb	11.65	1.128	8	Q_β	6.50		7.52	7.16	8.62	7.66
				B_n	3.28	3.28 (s)	3.86	3.38	3.21	3.74
^{136}Te	9.50	0	0.5 [i)]	Q_β	4.90		4.47	4.41	5.46	4.56
				B_n	3.72	3.72±0.10	4.02	3.84	3.74	4.06
^{137}I	12.99	1.152	5.4	Q_β	5.65	5.40 (s)	5.79	5.50	6.34	5.84
				B_n	3.86	3.86±0.03	4.45	3.99	4.01	4.38
^{138}I	13.94	1.974	2.5	Q_β	7.80		7.80	7.81	8.32	7.96
				B_n	5.93	5.93 (s)	5.86	5.92	5.49	5.81
^{139}I	14.65	1.152	10 [h)]	Q_β	6.10		6.67	6.33	7.26	6.78
				B_n	3.97	3.97 (s)	3.89	3.76	3.81	4.00
^{140}I	15.36	1.995	14 [j)]	Q_β	7.40		8.93	8.61	9.85	8.98
				B_n	5.34	5.34 (s)	5.35	5.67	5.51	5.49
^{141}I	18.23	1.152	30 [j)]	Q_β	5.50		7.42	7.13	8.28	7.66
				B_n	3.50		3.52	3.54	3.20	3.60
^{142}Cs	17.20	1.982	0.29 [k)]	Q_β	7.00	6.70 (s)	7.24	7.00	7.72	7.27
				B_n	5.87	5.87±0.15	6.20	6.25	6.24	6.11
^{143}Cs	18.01	1.139	1.13	Q_β	6.00		5.73	5.52	6.18	5.83
				B_n	4.31	4.31 (s)	4.03	4.12	3.98	4.21
^{144}Cs	18.47	2.107	1.1 [ℓ)]	Q_β	7.65		8.05	7.78	8.88	10.27
				B_n	5.86	5.86 (s)	6.16	6.00	6.29	6.01

Table 1 (continued)

Precursor for which the neutron spectra have been constructed by an extrapolation procedure

Precursor	a[a] MeV^{-1}	P[b] MeV	P_n[b] %		Q_β/B_n MeV Present work	Wapstra and Gove[c]	Garvey et al[d]	Myers and Swia-[e]	Liran and Zeldes[f]	Seeger and Howard[g]
^{93}Kr	12.62	1.095	1.9	Q_β	7.72[n]		8.15	7.45	8.64	8.13
				B_n	6.11	6.11(s)	6.30	6.89	6.21	6.53
^{96}Rb	13.55	2.419	12.7	Q_β	10.1[o]		10.76	9.70	11.10	10.44
				B_n	6.78		6.62	7.27	6.40	6.81
^{97}Rb	13.99	1.272	20	Q_β	8.01[o]		9.03	8.07	9.53	8.81
				B	4.22		3.92	4.62	3.99	4.34
^{97}Y	12.74	1.198	1.6	Q_β	6.10[c]	6.10(s)	5.35	4.65	5.67	5.44
				B_n	5.58	5.58±0.21	5.22	5.73	5.43	5.07
^{99}Y	13.69	1.198	1.2	Q_β	6.62[n]		6.51	5.84	6.84	6.52
				B_n	5.15	5.15(s)	4.44	5.38	4.91	5.09

a) Ref.[9]

b) If no other references are given: ref.[14] (except for the values within brackets which are estimated).

c) Ref.[13]. The symbol (s) indicates values deduced from systematics.

d) Ref.[17]

e) Ref.[18]

f) Ref.[19]

g) Ref.[20]

h) Ref.[21]

i) Ref.[22]

j) Ref.[23]

k) Ref.[24]

l) Ref.[25]

m) Ref.[30]

n) Average of mass formulas[17-20]

o) Extrapolated value

p) Ref.[29]

q) Ref.[45]

Table 2

Parameters describing the energy spectrum of the delayed neutrons

Precursor	Gross structure					Fine structure	
	ℓ	E_γ MeV	C_ℓ $keV^{-19/4}$	$k\Gamma_\gamma$	Intensity %	E_n MeV	Intensity %
^{79}Ga a)	1	0	$1.82x10^{-22}$	0.00010	0.67		
	3	0	$2.49x10^{-22}$	0.00066	0.33		
^{80}Ga a)	0	0.6	$1.50x10^{-20}$	0.0277	0.50		
	2	0	$4.39x10^{-22}$	0.0032	0.30		
	4	0	$3.09x10^{-21}$	0.0001	0.20		
^{81}Ga a)	1	0	$5.91x10^{-22}$	0.0001	6.77	0.08	0.38
						0.14	0.55
						0.24	0.34
						0.29	0.36
						0.33	0.80
						0.38	0.40
						0.44	0.18
						0.50	0.10
						0.56	0.12
^{85}As b)	1	1.455	$1.55x10^{-20}$	0.00010	3.0	0.11	0.3
						0.18	0.9
	3	0	$1.81x10^{-21}$	0.00017	10.2	0.51	2.5
						0.57	0.5
						0.65	1.1
						0.71	0.3
						0.91	0.8
						1.02	0.4
^{87}Br c)	1	0	$2.73x10^{-21}$	0.00010	1.04	0.13	0.40
						0.18	0.27
	3	0	$4.16x10^{-21}$	0.0031	0.13	0.25	0.31
						0.44	0.11
						0.64	0.04
^{88}Br d)	1	0	$4.45x10^{-22}$	0.00010	3.86	0.08	0.41
						0.13	0.18
						0.39	0.08
						0.54	0.05
						0.67	0.02

Table 2(continued)

Precursor	Gross structure					Fine structure	
	ℓ	E_γ MeV	C_ℓ keV$^{-19/4}$	$k\Gamma_\gamma$	Intensity %	E_n MeV	Intensity %
^{89}Br e)	1	0	$3.91\mathrm{x}10^{-22}$	0.00028	4.52	0.13	0.18
						0.18	0.13
	3	0	$5.28\mathrm{x}10^{-22}$	0.00040	3.01	0.27	0.11
						0.39	0.10
						0.62	0.25
						0.68	0.18
						0.74	0.09
						0.80	0.03
^{90}Br d)	1	0	$1.75\mathrm{x}10^{-23}$	0.00012	6.0		
	1	1.0	$1.17\mathrm{x}10^{-22}$	0.00041	6.0		
^{91}Br e)	1	0	$1.43\mathrm{x}10^{-22}$	0.0001	5.1		
	3	0	$1.51\mathrm{x}10^{-22}$	0.00026	3.2		
^{93}Rb e)	1	0	$7.86\mathrm{x}10^{-23}$	0.0001	0.820	0.11	0.046
						0.23	0.030
	3	0	$4.44\mathrm{x}10^{-23}$	0.0006	0.176	0.27	0.032
						0.32	0.025
						0.38	0.025
						0.46	0.024
						0.52	0.013
						0.78	0.009
^{94}Rb a)	1	1.0	$8.33\mathrm{x}10^{-23}$	0.00010	7.4		
	3	0	$3.13\mathrm{x}10^{-24}$	0.00026	2.2		
^{95}Rb a)	1	0.6	$6.90\mathrm{x}10^{-24}$	0.00010	5.0		
	3	0	$2.59\mathrm{x}10^{-24}$	0.00013	3.4		
^{129}In a)	1	1.169	$8.36\mathrm{x}10^{-21}$	0.00012	3.0		
	2	1.169	$1.48\mathrm{x}10^{-18}$	1.0	3.0		
	3	0	$2.88\mathrm{x}10^{-22}$	0.0240	2.5		
	4	0	$2.39\mathrm{x}10^{-20}$	0.149	1.5		
^{130}In a)	0	1.044	$3.38\mathrm{x}10^{-21}$	0.0169	3.5		
	2	1.044	$2.95\mathrm{x}10^{-19}$	1.0	3.0		
	3	0.035	$1.80\mathrm{x}10^{-22}$	0.0275	2.0		
	4	0	$1.40\mathrm{x}10^{-21}$	0.0100	1.5		
^{134}Sn c)	0	1.0	$1.14\mathrm{x}10^{-21}$	0.0066	5.1	0.50	3.4
	2	0	$3.71\mathrm{x}10^{-22}$	0.0115	8.5		

Table 2 (continued)

Precursor	Gross structure					Fine structure	
	ℓ	E_γ MeV	C_ℓ keV$^{-19/4}$	$k\Gamma_\gamma$	Intensity %	E_n MeV	Intensity %
^{135}Sb c)	0	1.278	2.89×10^{-22}	0.0036	4.77	0.17	0.09
						0.24	0.06
	2	0	1.65×10^{-23}	0.0013	1.19	0.28	0.05
						0.40	0.09
	4	0	1.51×10^{-23}	0.00045	0.60	0.47	0.08
						0.51	0.05
						0.55	0.06
						0.61	0.08
						0.83	0.09
						0.95	0.04
						0.98	0.10
						1.04	0.26
						1.20	0.13
						1.30	0.08
						1.45	0.18
^{136}Te c)	0	0.8	3.78×10^{-19}	0.0532	0.207	0.09	0.099
						0.25	0.008
	2	0	1.95×10^{-20}	1.35	0.083	0.31	0.013
						0.43	0.052
						0.46	0.025
						0.53	0.006
						0.58	0.007
^{137}I c)	0	1.313	4.82×10^{-20}	0.0364	0.52	0.08	0.15
						0.16	0.10
	2	0	7.84×10^{-22}	0.0304	2.23	0.27	0.18
						0.32	0.05
	4	0	3.42×10^{-22}	0.0001	0.65	0.38	0.42
						0.42	0.14
						0.48	0.20
						0.51	0.26
						0.58	0.19
						0.75	0.09
						0.85	0.11
						0.95	0.04
						1.14	0.04

Table 2 (continued)

Precursor	Gross structure					Fine structure	
	ℓ	E_γ MeV	C_ℓ $keV^{-19/4}$	$k\Gamma_\gamma$	Intensity %	E_n MeV	Intensity %
$^{138}I^{d)}$	0	0	$2.38x10^{-23}$	0.0036	2.41	0.38	0.06
						0.57	0.03
$^{139}I^{e)}$	0	0.593	$2.40x10^{-22}$	0.0051	4.16	0.13	0.06
						0.19	0.06
	2	0	$4.62x10^{-23}$	0.0144	1.66	0.28	0.08
						0.35	0.11
						0.42	0.10
						0.48	0.08
						0.57	0.17
						1.04	0.02
$^{140}I^{d)}$	0	1.0	$5.43x10^{-22}$	0.0107	5.6		
	2	0	$9.02x10^{-23}$	0.0173	8.4		
$^{141}I^{e)}$	0	1.0	$2.38x10^{-21}$	0.0104	12.3	0.16	1.7
						0.22	2.0
	2	0	$1.78x10^{-22}$	0.0122	8.2	0.30	2.3
						0.34	1.1
						0.39	1.3
						0.45	0.6
						0.55	0.5
$^{142}Cs^{d)}$	0	0.49	$1.36x10^{-23}$	0.0097	0.21		
	2	0	$2.10x10^{-22}$	0.104	0.08		
$^{143}Cs^{e)}$	0	0.835	$1.42x10^{-22}$	0.0142	0.82	0.18	0.04
	2	0	$3.88x10^{-24}$	0.0310	0.18	0.22	0.05
						0.31	0.02
						0.35	0.02
$^{144}Cs^{d)}$	0	0.50	$5.51x10^{-24}$	0.0070	0.86		
	2	0	$8.84x10^{-25}$	0.0266	0.24		

Table 2 (continued)

Precursors for which the neutron spectra have been constructed by an extra-polation procedure

Precursor	Gross structure					Fine structure	
	ℓ	E_γ MeV	C_ℓ keV$^{-19/4}$	$k\Gamma_\gamma$	Intensity %	E_n MeV	Intensity %
^{93}Kr	1	0	2.07×10^{-23}	0.00010	1.6		
	3	0	1.05×10^{-23}	0.00063	0.3		
^{96}Rb	1	1.0	4.09×10^{-24}	0.00010	9.8		
	3	0	4.80×10^{-25}	0.00010	2.9		
^{97}Rb	1	0.6	5.63×10^{-24}	0.00010	11.9		
	3	0	3.01×10^{-24}	0.00010	8.1		
^{97}Y	1	0	4.35×10^{-20}	0.00019	1.3		
	3	0	7.72×10^{-20}	0.00010	0.3		
^{99}Y	1	0	5.40×10^{-23}	0.00010	1.0		
	3	0	3.37×10^{-23}	0.00075	0.2		

a) Experimental data from ref.[26)]
b) " " " ref.[27)]
c) " " " ref.[2)]
d) " " " ref.[4)]
e) " " " ref.[3)]

Table 3. Transmission coefficients for neutrons. Emitting nucleus: ^{137}Xe

E_n keV	T_o	T_1	T_2	T_3	T_4	T_5
4	0.931, -1	0.804, -3	0.693, -6	0.350, -9	0.711, -13	~0
10	0.143	0.312, -2	0.683, -5	0.861, -8	0.284, -11	0.213, -13
20	0.196	0.854, -2	0.384, -4	0.968, -7	0.637, -10	0.568, -13
40	0.266	0.227, -1	0.215, -3	0.108, -5	0.143, -8	0.148, -11
80	0.355	0.566, -1	0.119, -2	0.119, -4	0.321, -7	0.646, -10
160	0.463	0.128	0.646, -2	0.129, -3	0.714, -6	0.284, -8
214	0.514	0.172	0.130, -1	0.344, -3	0.261, -5	0.137, -7
320	0.587	0.248	0.331, -1	0.131, -2	0.156, -4	0.121, -6
640	0.717	0.403	0.148	0.119, -1	0.328, -3	0.482, -5
1280	0.835	0.552	0.465	0.799, -1	0.645, -2	0.170, -3
2560	0.911	0.651	0.842	0.290	0.106	0.468, -2
5120	0.912	0.681	0.969	0.514	0.742	0.841, -1
7928	0.817	0.678	0.929	0.609	0.978	0.348

(0.931, -1 equals 0.931 x 10^{-1}, etcetera)

Table 4. Transmission coefficients for neutrons. Emitting nucleus: ^{87}Kr

E_n keV	T_o	T_1	T_2	T_3	T_4	T_5
4	0.534, -1	0.812, -3	0.424, -6	0.137, -9	0.355, -13	$\sim$ 0
10	0.831, -1	0.318, -2	0.417, -5	0.339, -8	0.931, -12	$\sim$ 0
20	0.115	0.887, -2	0.234, -4	0.382, -7	0.202, -10	0.284, -13
40	0.159	0.243, -1	0.130, -3	0.431, -6	0.453, -9	0.433, -12
80	0.216	0.644, -1	0.716, -3	0.483, -5	0.101, -7	0.183, -10
160	0.290	0.158	0.380, -2	0.537, -4	0.223, -6	0.816, -9
214	0.326	0.223	0.751, -2	0.147, -3	0.810, -6	0.400, -8
320	0.380	0.341	0.187, -1	0.585, -3	0.478, -5	0.359, -7
640	0.482	0.600	0.783, -1	0.614, -2	0.972, -4	0.154, -5
1280	0.586	0.842	0.238	0.583, -1	0.177, -2	0.623, -4
2560	0.675	0.977	0.469	0.380	0.255, -1	0.228, -2
5120	0.728	0.988	0.648	0.905	0.219	0.672, -1
7928	0.746	0.945	0.719	0.974	0.528	0.370

(0.534, -1 equals 0.534 x 10^{-1}, etcetera)

Table 5. Comparison between experimentally determined Q_β -values and results from the present work

Precursor	Experimental MeV	This work MeV
^{87}Br	6.84±0.12 [a]	6.60
^{88}Br	≳ 8.2 ±0.5 [b]	8.55
^{93}Rb	5.75±0.10 [c]	6.72
	7.23±0.10 [e]	
^{137}I	5.5 ±0.2 [b]	5.65
^{138}I	7.3 ±0.5 [b]	7.80
^{139}I	≥ 6.0 ±0.4 [b]	6.10
^{142}Cs	6.77±0.2 [d]	7.00
	6.89±0.06 [f]	
^{143}Cs	5.65±0.2 [d]	6.00
^{144}Cs	8.1 ±0.3 [d]	7.65

a) Ref. [31]
b) Ref. [30]
c) Ref. [32]
d) Ref. [33]
e) Ref. [44]
f) Ref. [46]

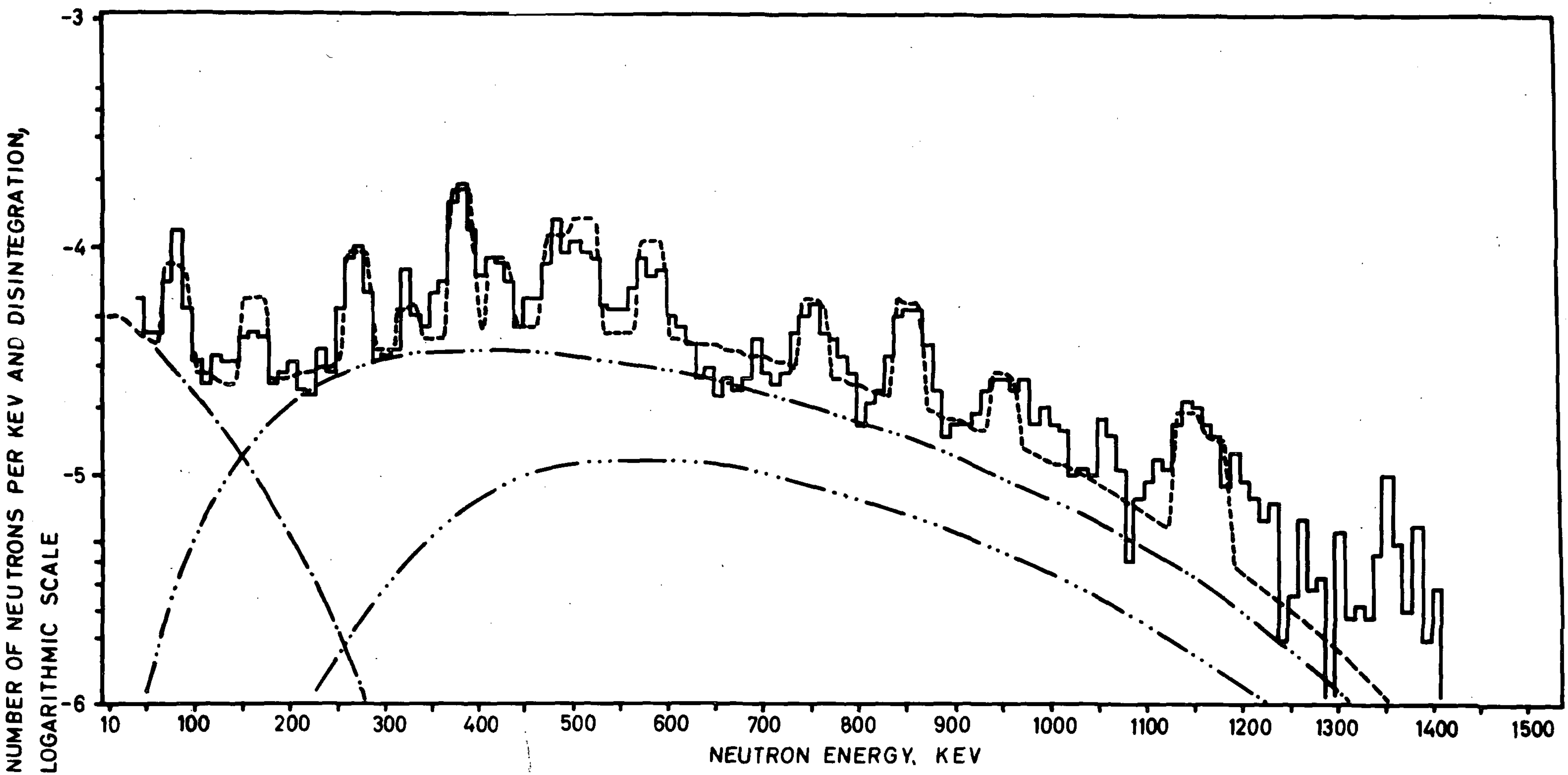

Fig. 1. Experimental and calculated delayed-neutron spectra for the precursor ^{137}I.
Histogram: Experimental spectrum[2)]
Dashed curve: Calculated spectrum
Dash-dot curve: s-wave component
Dash-dot-dot curve: d-wave component
Dash-dot-dot-dot curve: g-wave component

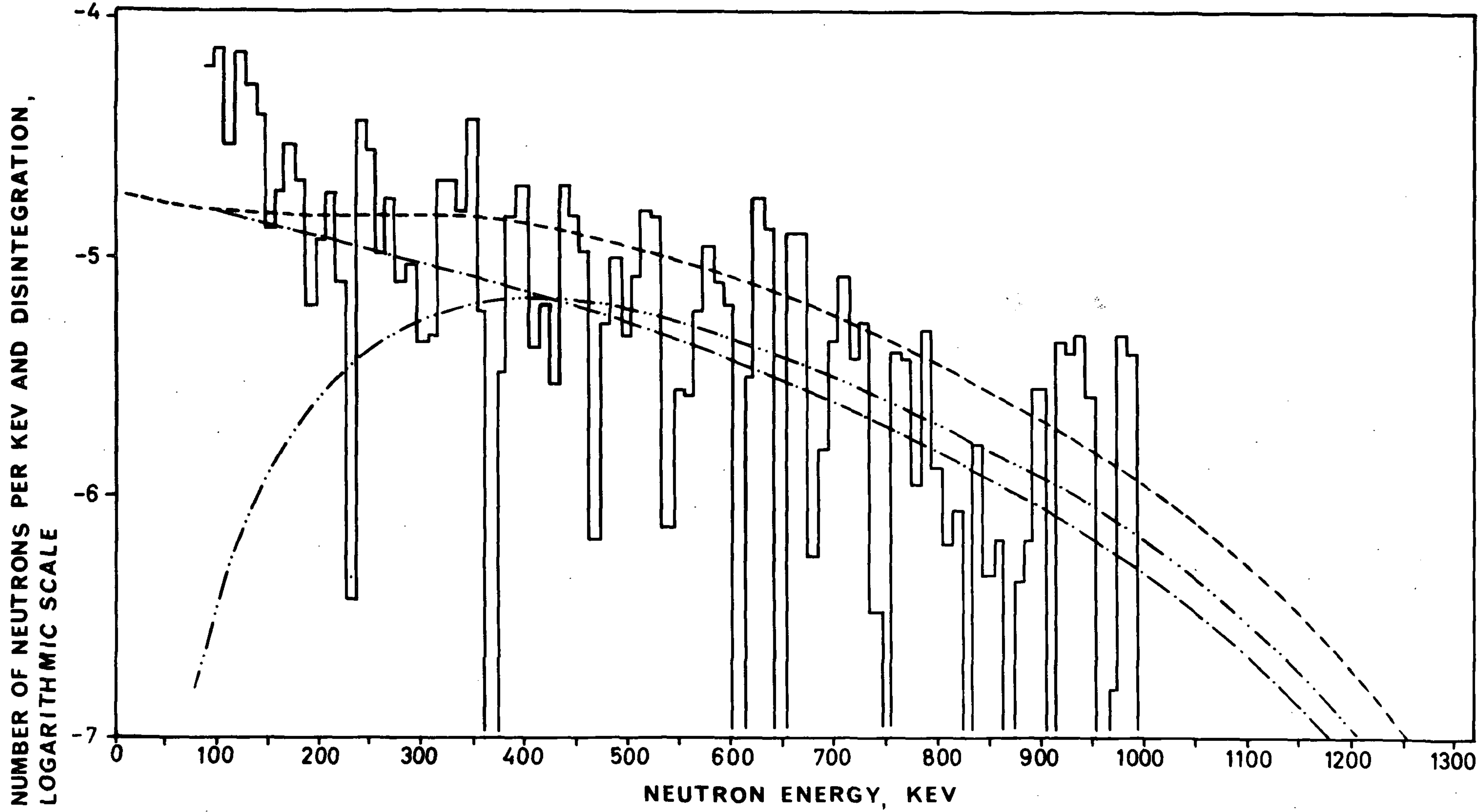

Fig. 2. Experimental and calculated delayed-neutron spectra for the precursor ^{79}Ga.
Histogram: Experimental spectrum[26)]
Dashed curve: Calculated spectrum
Dash-dot curve: p-wave component
Dash-dot-dot curve: f-wave component

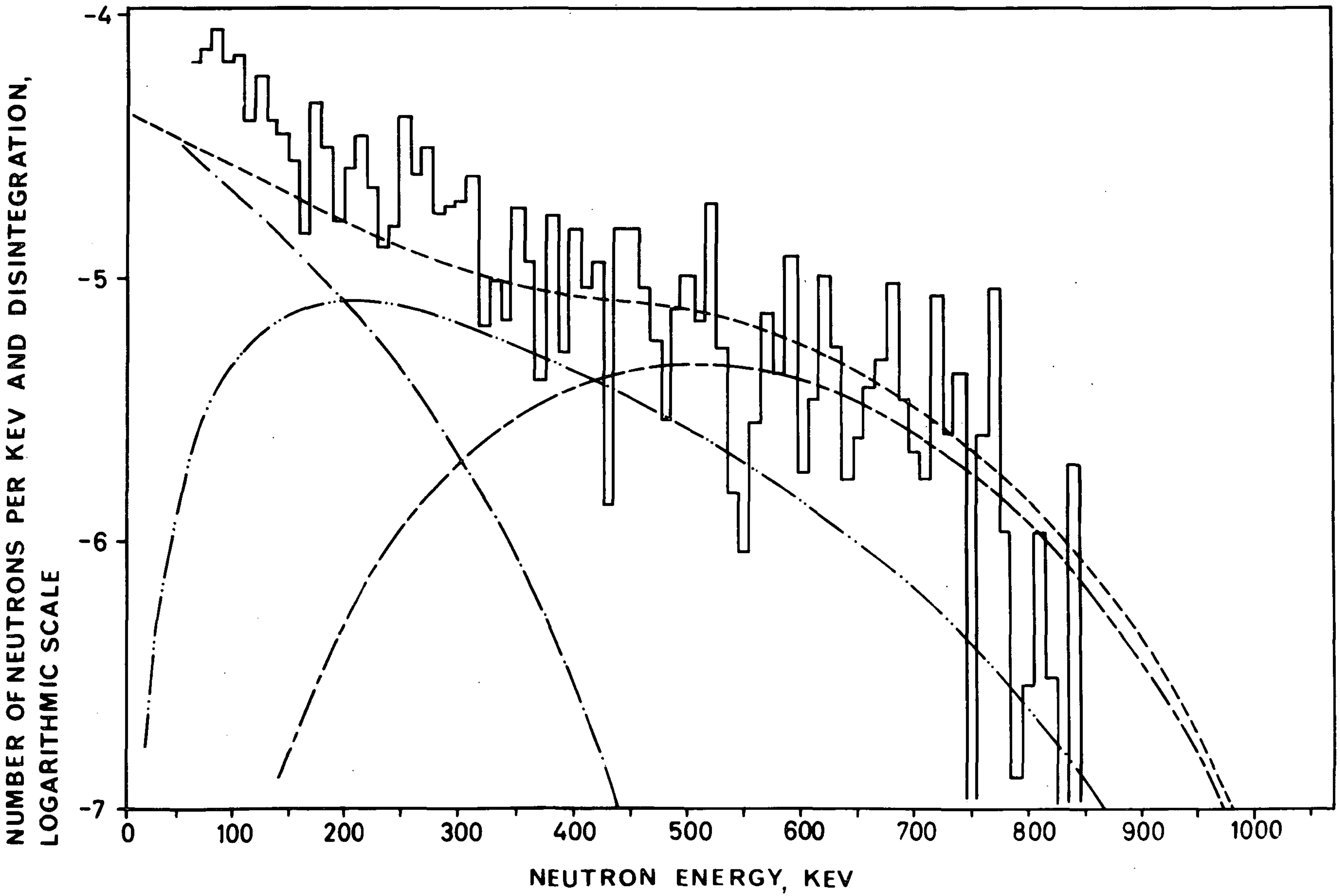

Fig. 3. Experimental and calculated delayed-neutron spectra for the precursor ^{80}Ga
Histogram: Experimental spectrum[26)]
Dashed curve: Calculated spectrum
Dash-dot-dot curve: d-wave component
Large dash-small dash curve: g-wave component
Dash-dot curve: s-wave component feeding a hypothetical excited level at 600 keV

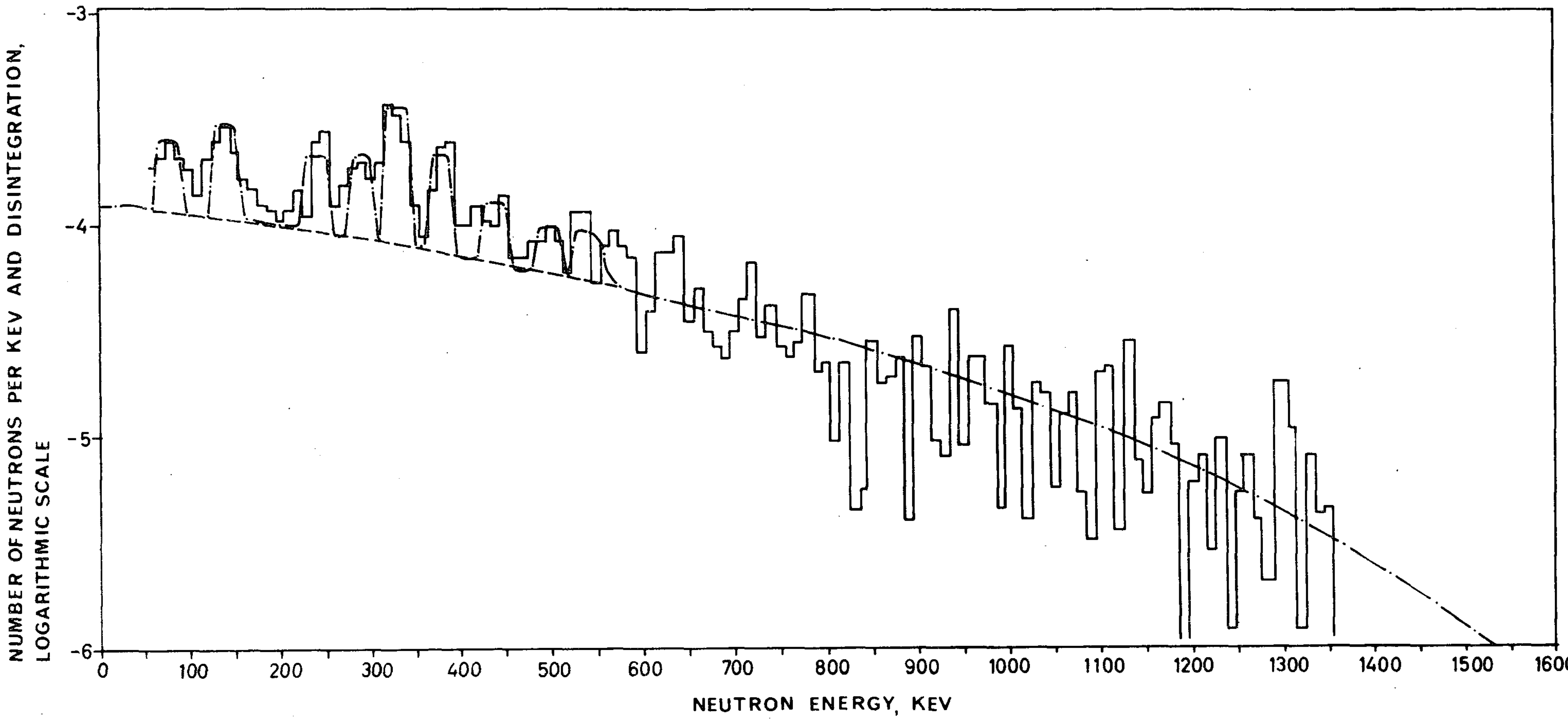

Fig. 4. Experimental and calculated delayed-neutron spectra for the precursor ^{81}Ga.
Histogram: Experimental spectrum[26)]
Dash-dot curve: Calculated spectrum
Dashed curve: p-wave component

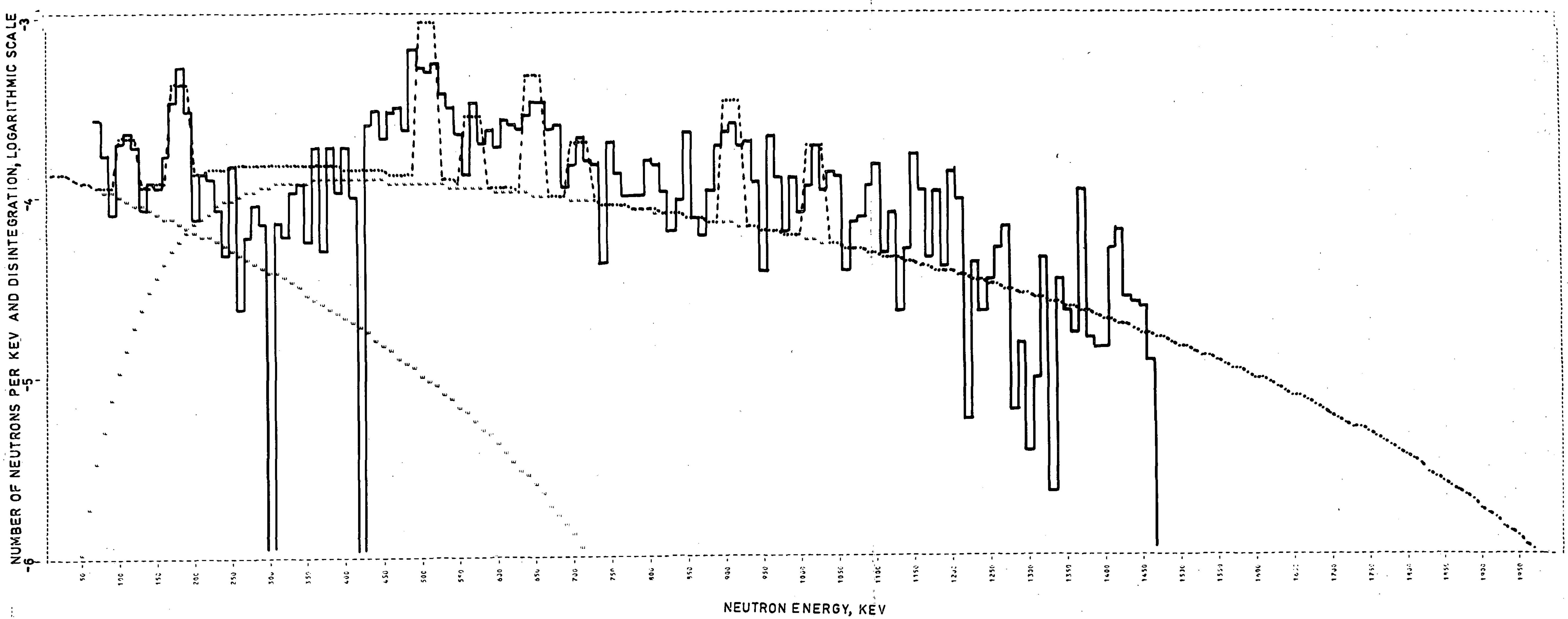

Fig. 5. Experimental and calculated delayed-neutron spectra for the precursor ^{85}As
Histogram: Experimental spectrum[27)]
Dotted curve: Calculated spectrum
Curve denoted by E: p-wave component to the level at 1455 keV in ^{84}Se
Curve denoted by F: f-wave component

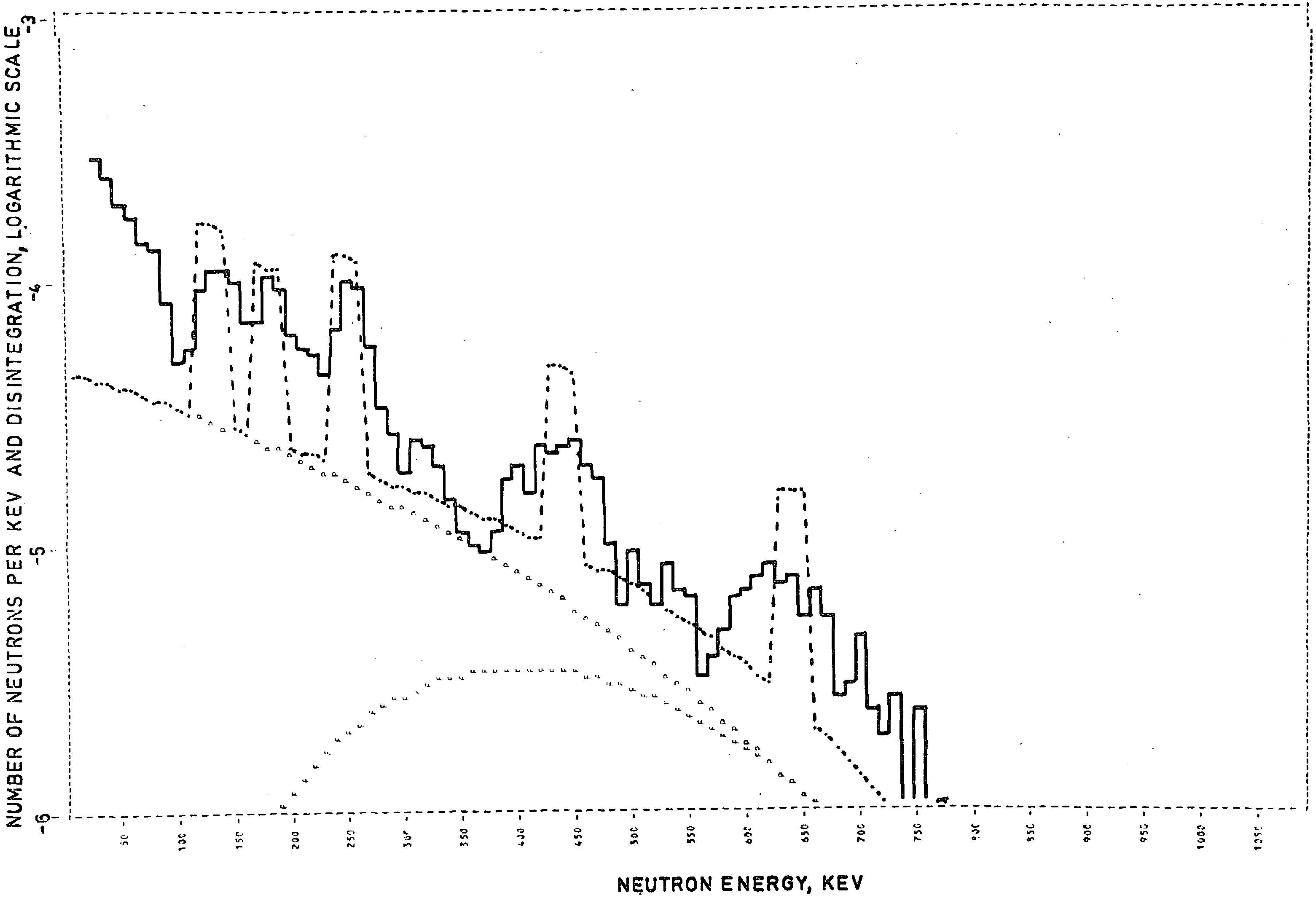

Fig. 6. Experimental and calculated delayed-neutron spectra from the precursor ^{87}Br.
Histogram: Experimental spectrum[2)]
Dotted curve: Calculated spectrum
Curve denoted by P: p-wave component
Curve denoted by F: f-wave component

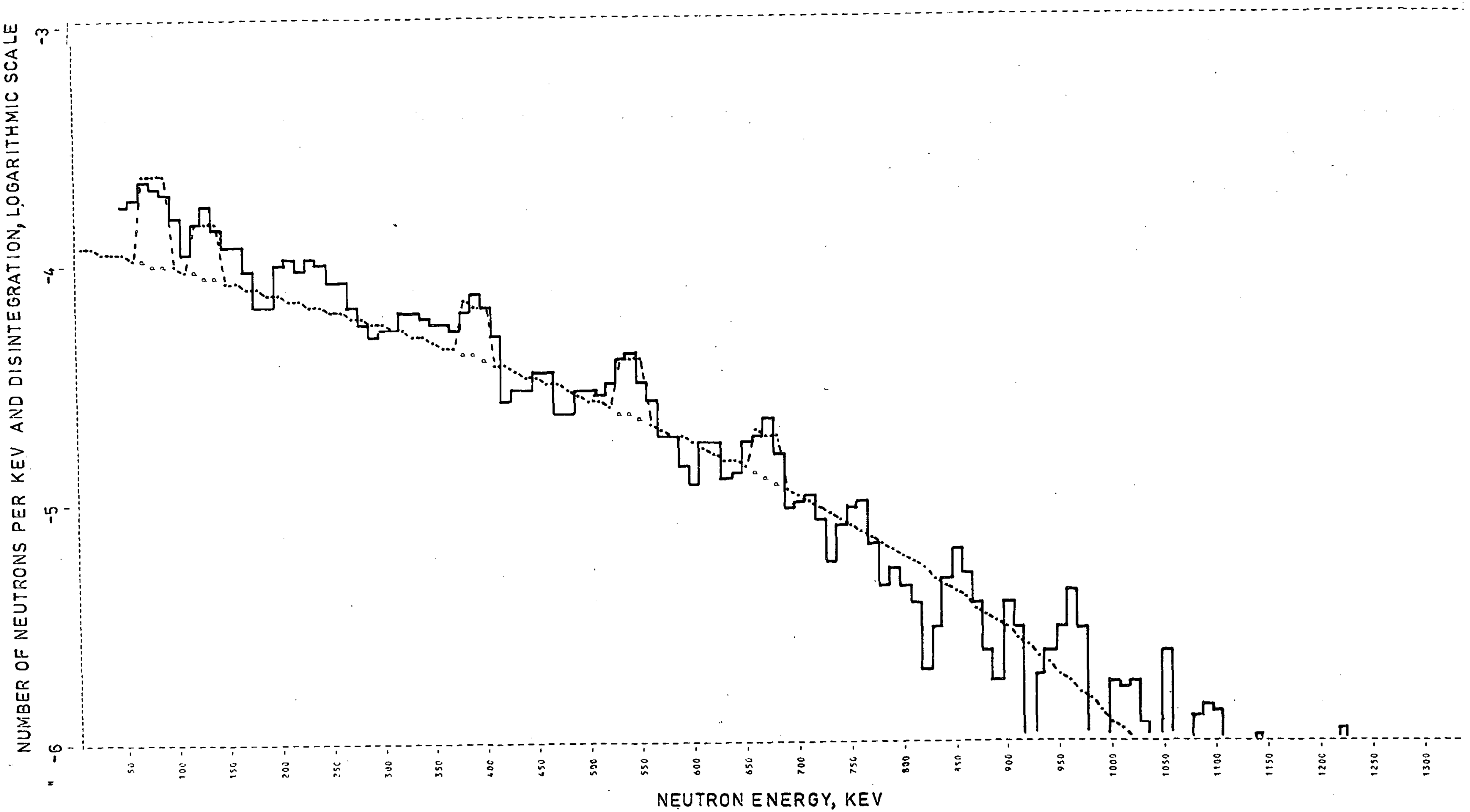

Fig. 7. Experimental and calculated delayed-neutron spectrum for the precursor ^{88}Br.
Histogram: Experimental spectrum[4)]
Dotted curve: Calculated spectrum
Curve denoted by P: p-wave component

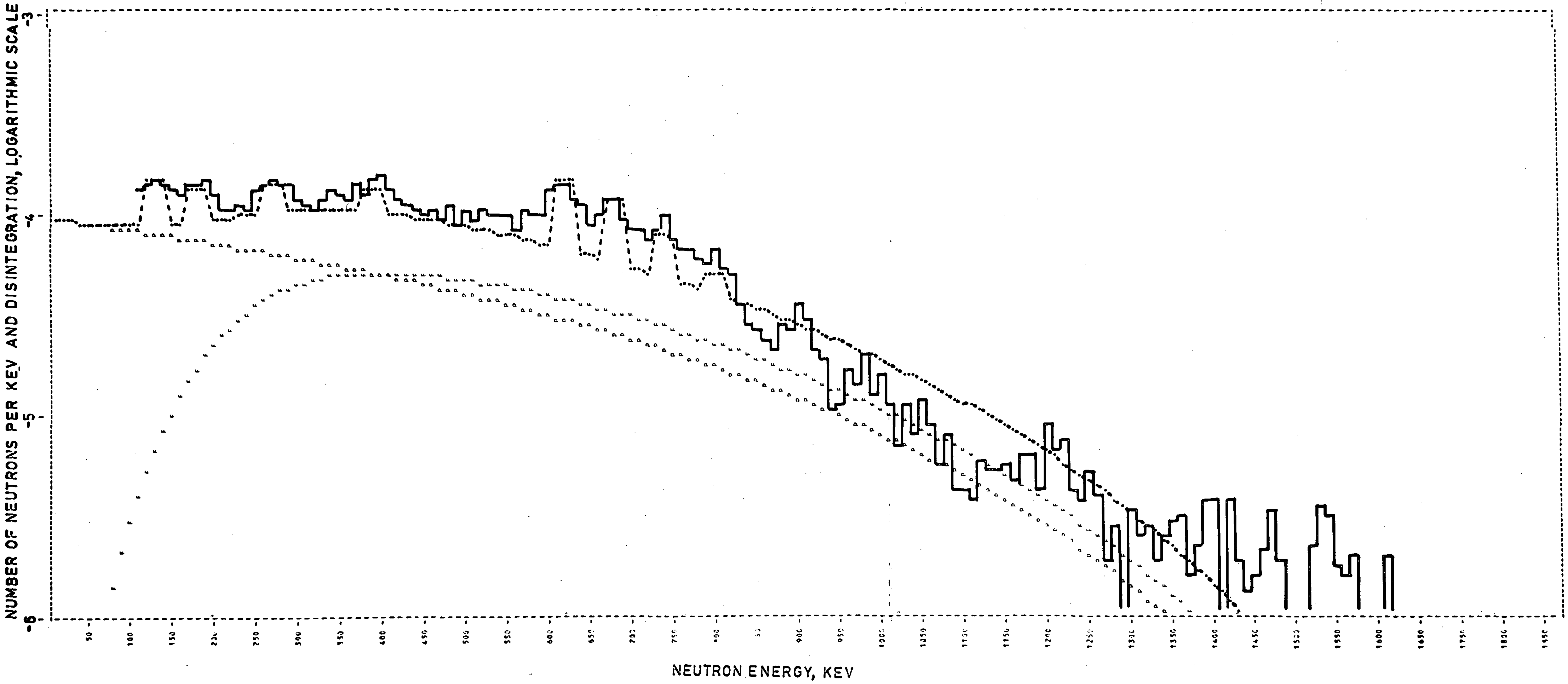

Fig. 8. Experimental and calculated delayed-neutron spectra for the precursor ^{89}Br
Histogram: Experimental spectrum[3)]
Dotted curve: Calculated spectrum
Curve denoted by P: p-wave component
Curve denoted by F: f-wave component

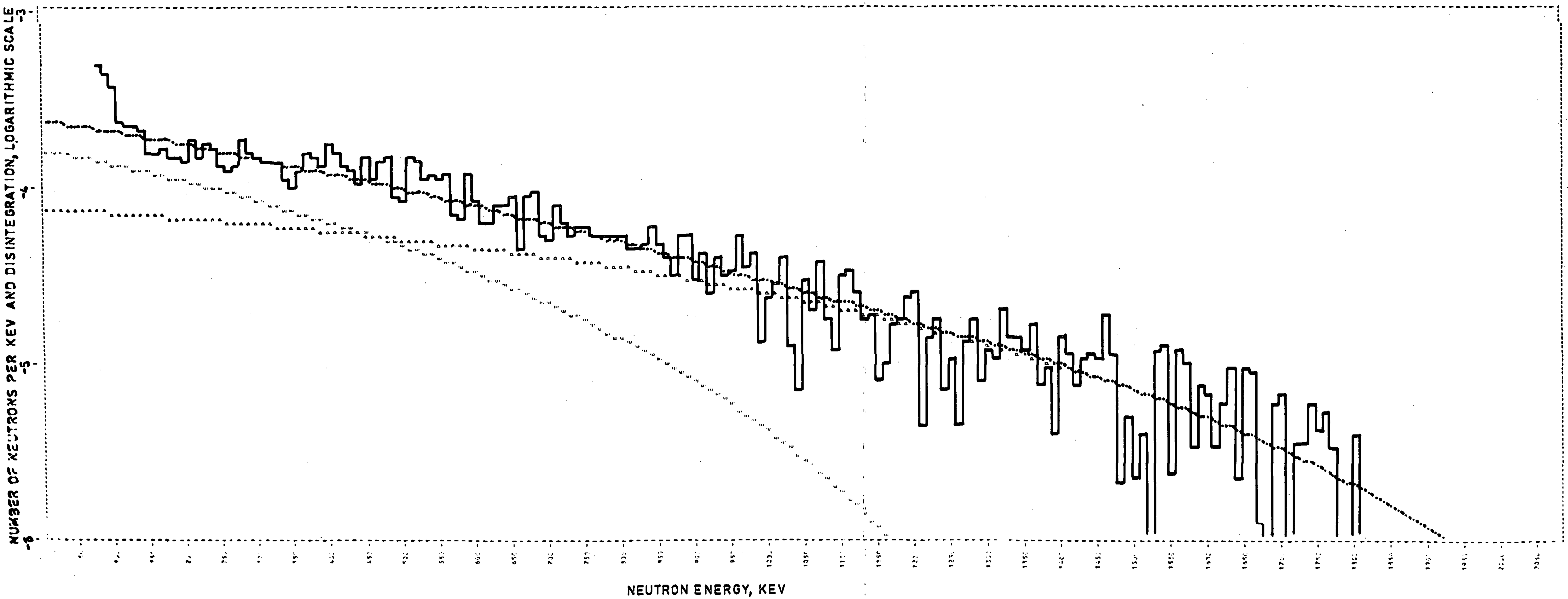

Fig. 9. Experimental and calculated delayed-neutron spectra for the precursor ^{90}Br
Histogram: Experimental spectrum[4)]
Dotted curve: Calculated spectrum
Curve denoted by E: p-wave component to a hypothetical level at 1.0 MeV in ^{89}Kr
Curve denoted by P: p-wave component

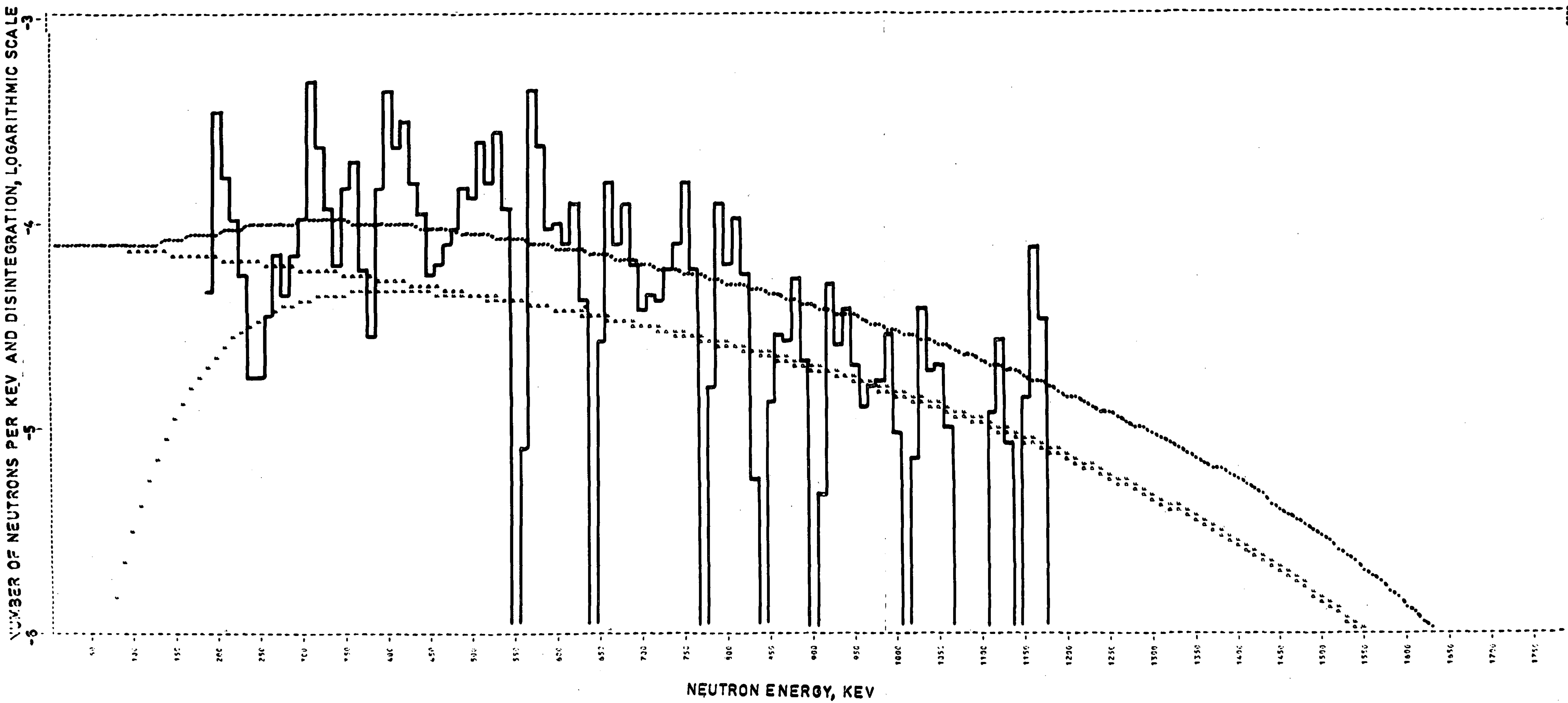

Fig. 10. Experimental and calculated delayed-neutron spectra for the precursor ^{91}Br
Histogram: Experimental spectrum[3)]
Dotted curve: Calculated spectrum
Curve denoted by P: p-wave component
Curve denoted by F: f-wave component

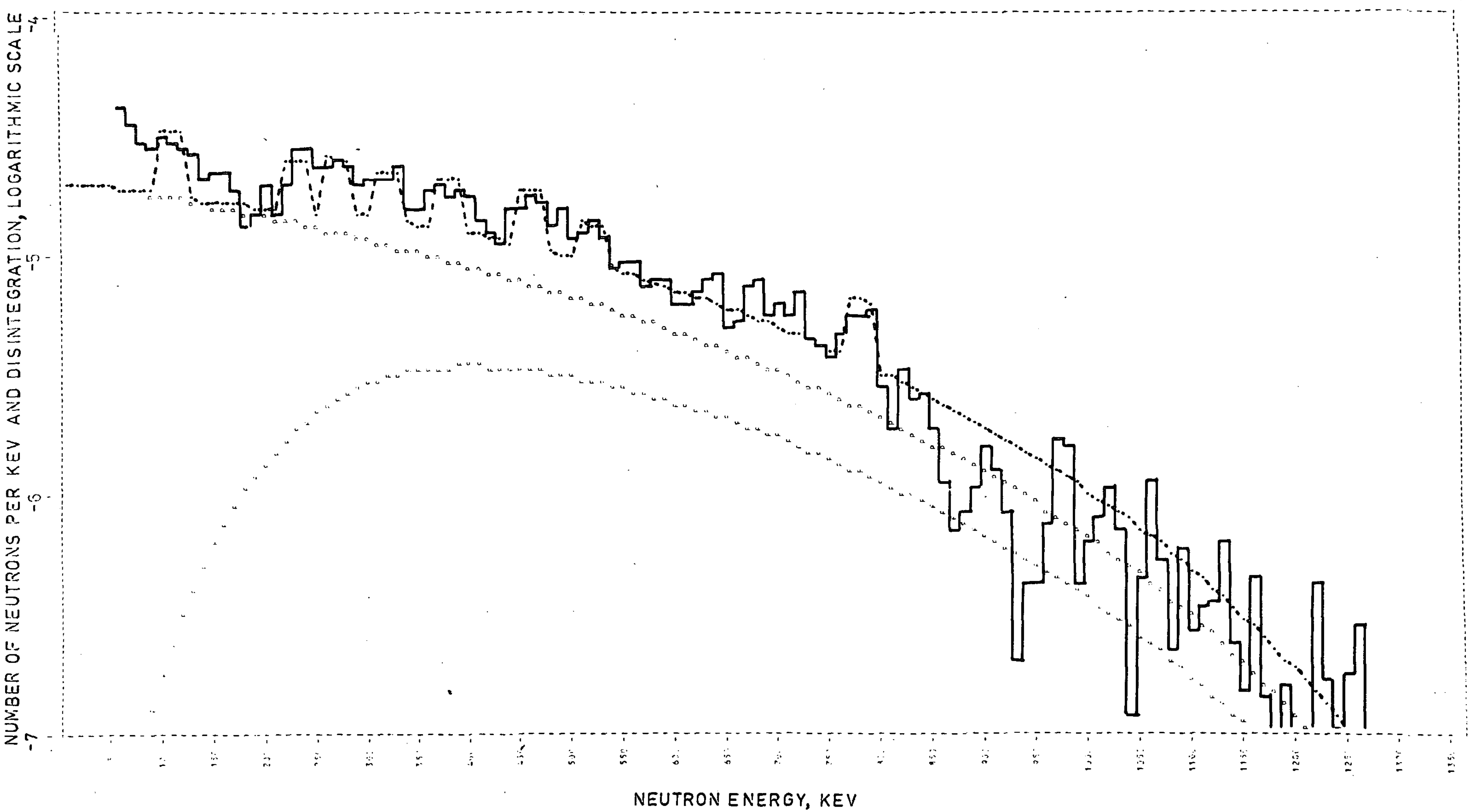

Fig. 11. Experimental and calculated delayed-neutron spectrum for the precursor ^{93}Rb
Histogram: Experimental spectrum[3)]
Dotted curve: Calculated spectrum
Curve denoted by P: p-wave component
Curve denoted by F: f-wave component

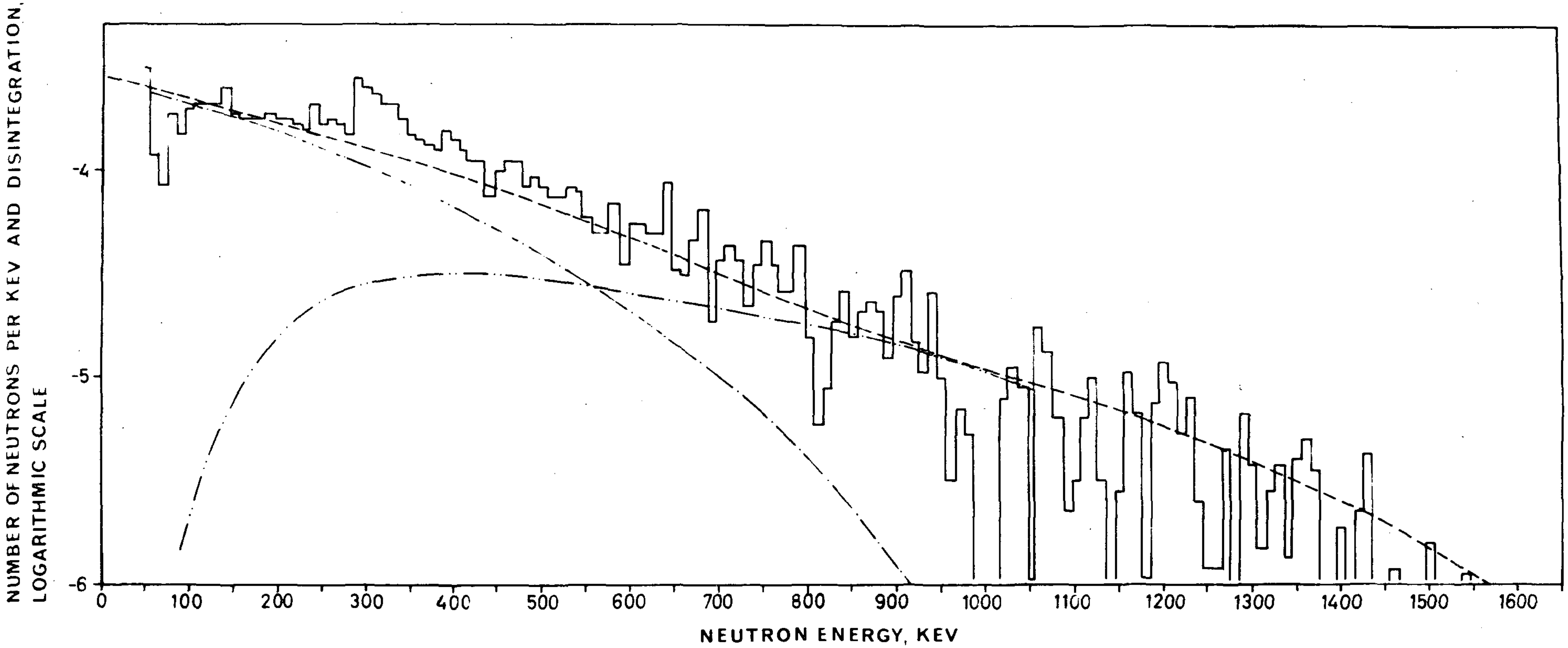

Fig. 12. Experimental and calculated delayed-neutron spectra for the precursor ^{94}Rb.
Histogram: Experimental spectrum[26)]
Dashed curve: Calculated spectrum
Dash-dot curve: p-wave component feeding a hypothetical excited level at 1 MeV
Dash-dot-dot curve: f-wave component

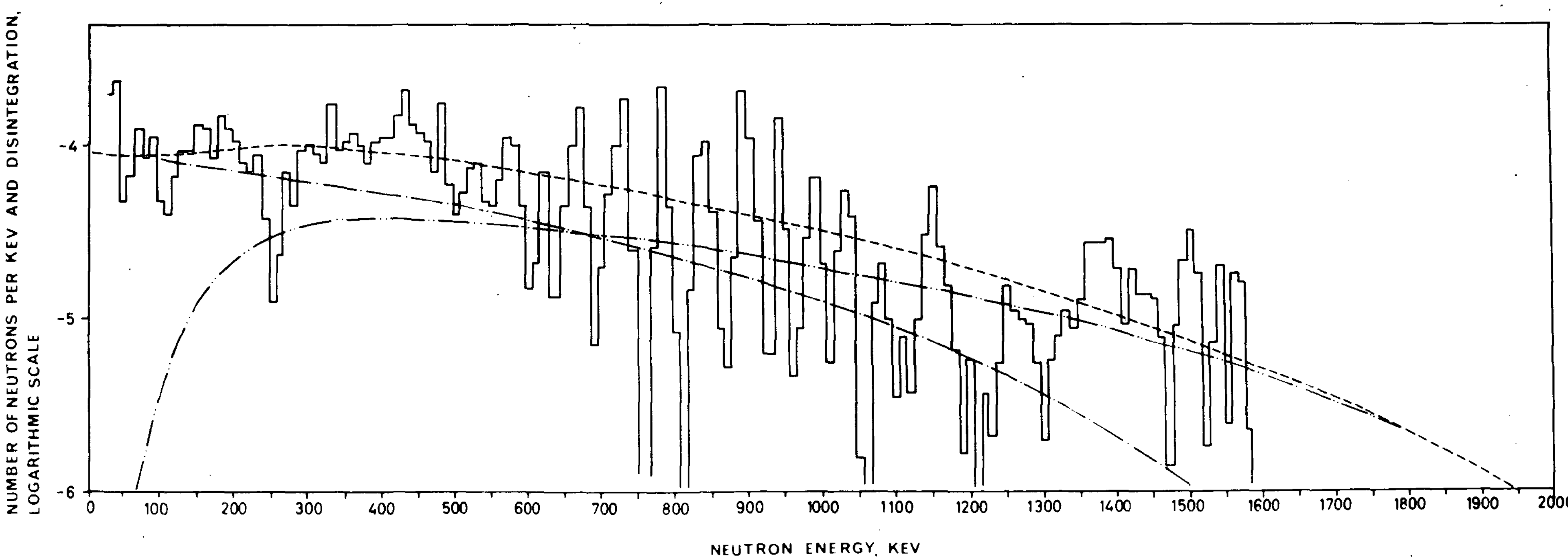

Fig. 13. Experimental and calculated delayed-neutron spectra for the precursor ^{95}Rb.
Histogram: Experimental spectrum[26)]
Dashed curve: Calculated spectrum
Dash-dot curve: p-wave component feeding a hypothetical excited level at 600 keV
Dash-dot-dot curve: f-wave component

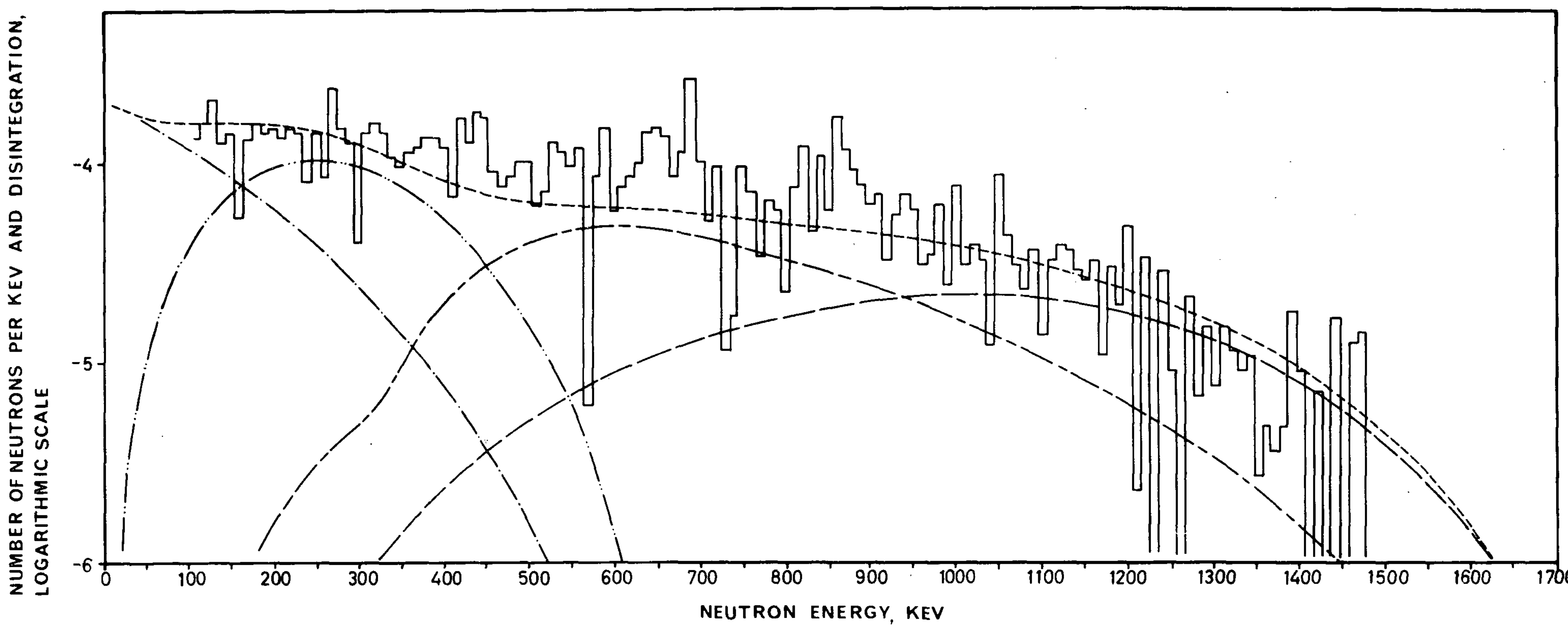

Fig. 14. Experimental and calculated delayed-neutron spectra for the precursor ^{129}In.
Histogram: Experimental spectrum[26)]
Dashed curve: Calculated spectrum
Dash-dot curve: p-wave component feeding an excited level at 1169 keV
Dash-dot-dot curve: d-wave component feeding an excited level at 1169 keV
Large dash-small dash curve: f-wave component
Large dash curve: g-wave component

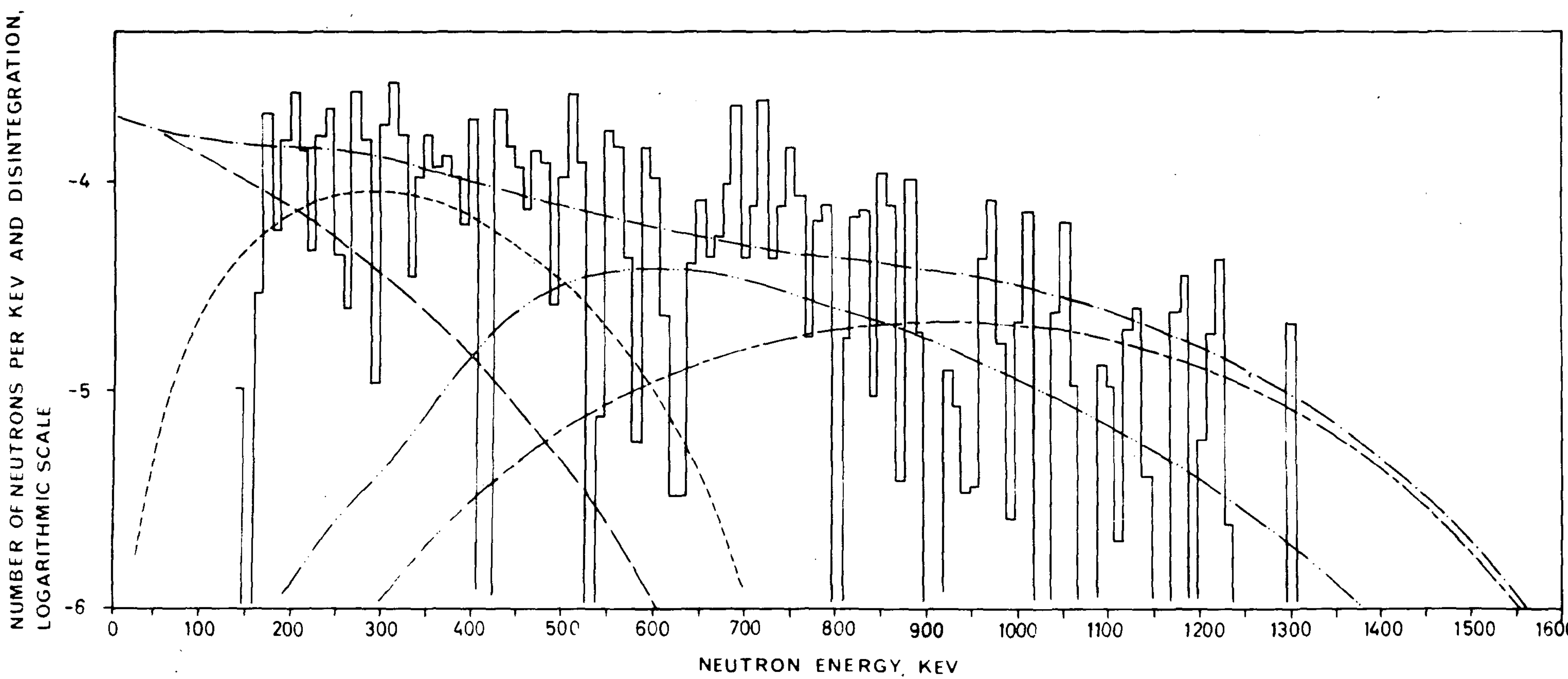

Fig. 15. Experimental and calculated delayed-neutron spectra for the precursor ^{130}In.
Histogram: Experimental spectrum[26)]
Dash-dot curve: Calculated spectrum
Large dash curve: s-wave component feeding an excited level at 1044 keV
Small dash curve: d-wave component feeding an excited level at 1044 keV
Dash-dot-dot curve: f-wave component
Large dash-small dash curve: g-wave component

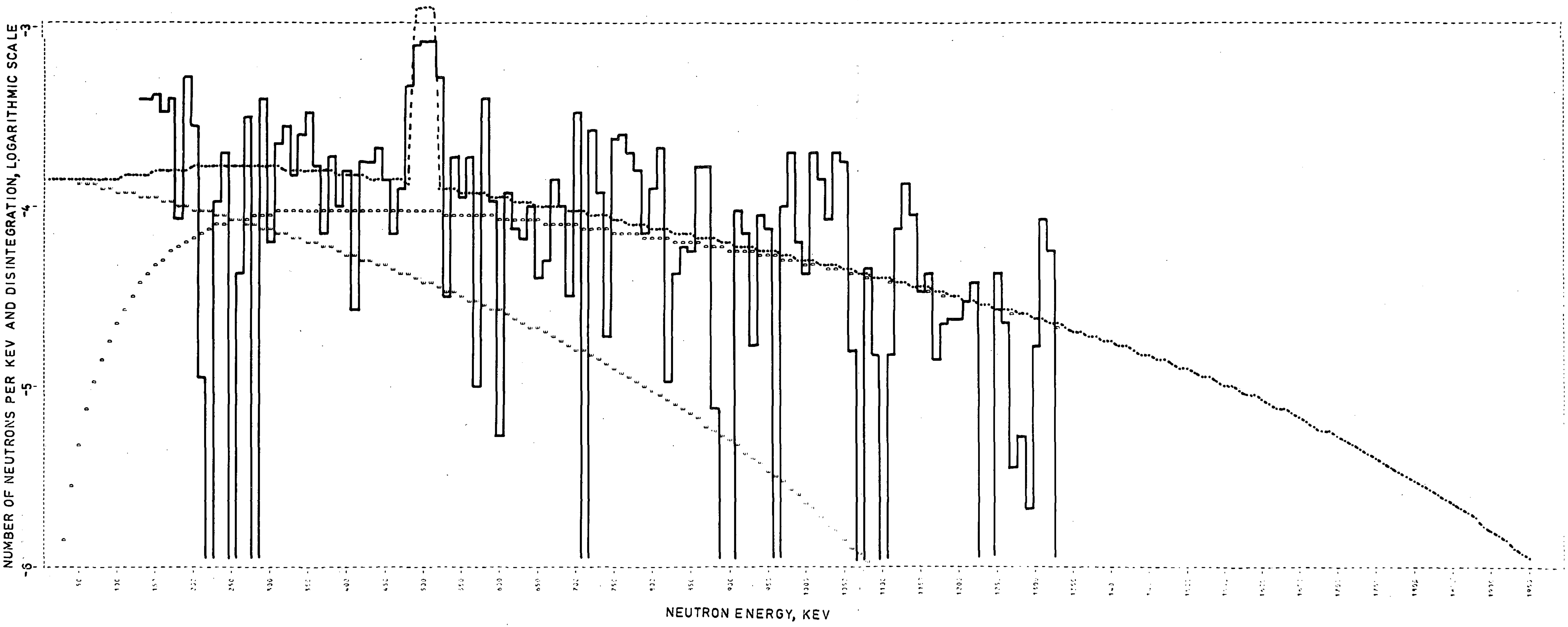

Fig. 16. Experimental and calculated delayed-neutron spectra for the precursor ^{134}Sn
Histogram: Experimental spectrum[2)]
Dotted curve: Calculated spectrum
Curve denoted by E: s-wave component to a hypothetical level at 1.0 MeV in ^{133}Sb
Curve denoted by D: d-wave component

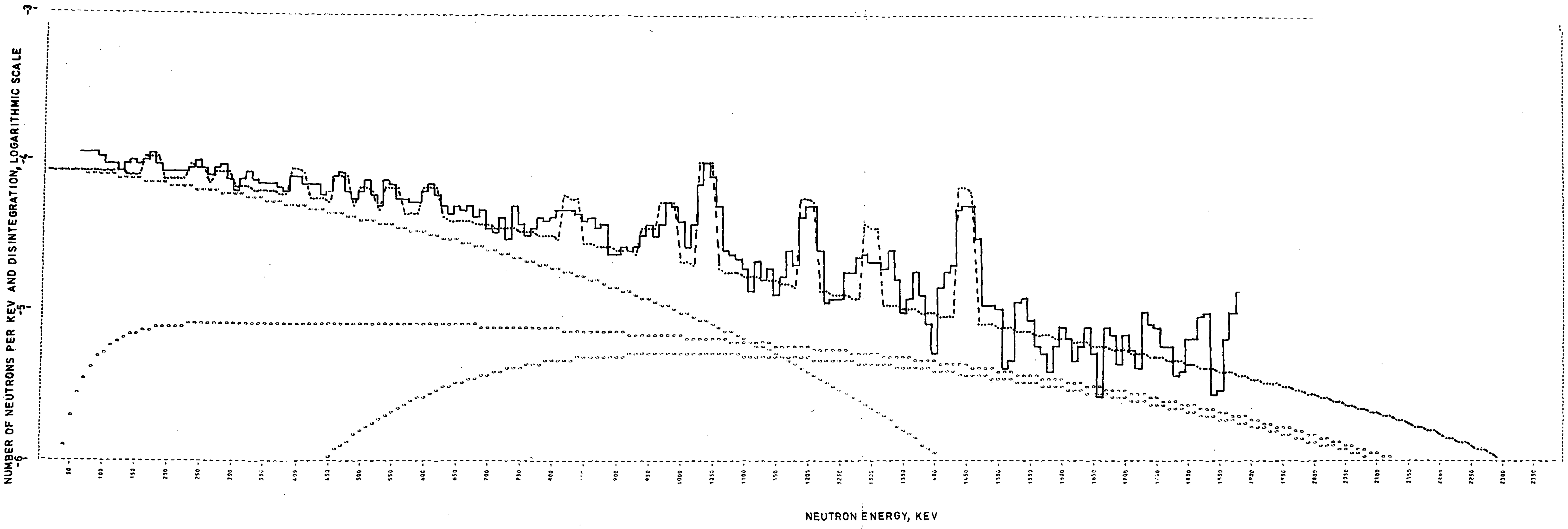

Fig. 17. Experimental and calculated delayed-neutron spectra for the precursor ^{135}Sb
Histogram: Experimental spectrum[2)]
Dotted curve: Calculated spectrum
Curve denoted by E: s-wave component to the level at 1278 keV in ^{134}Te
Curve denoted by D: d-wave component
Curve denoted by G: g-wave component

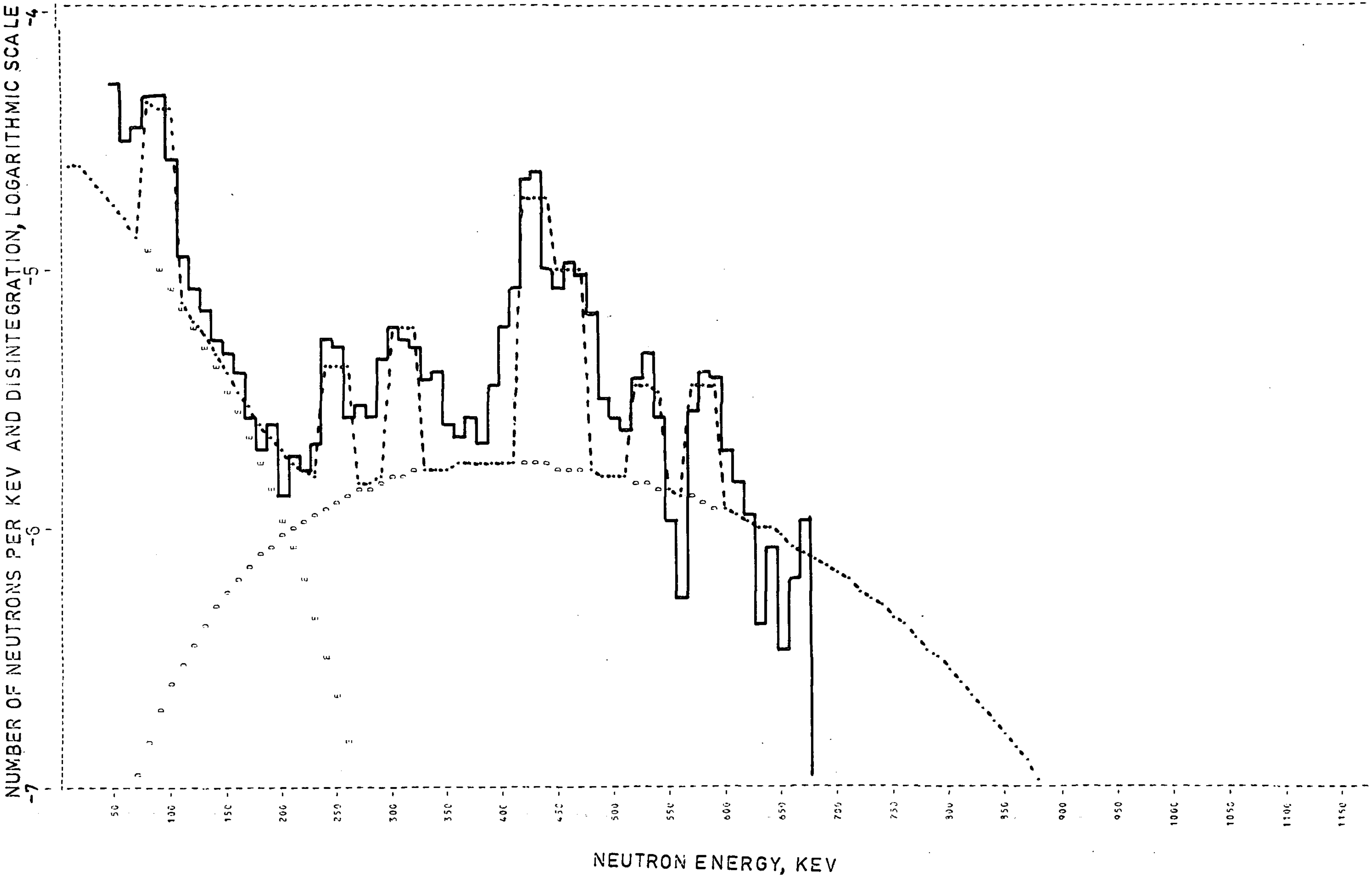

Fig. 18. Experimental and calculated delayed-neutron spectra for the precursor ^{136}Te
Histogram: Experimental spectrum[2)]
Dotted curve: Calculated spectrum
Curve denoted by E: s-wave component to a hypothetical level at 0.8 MeV in ^{135}I
Curve denoted by D: d-wave component

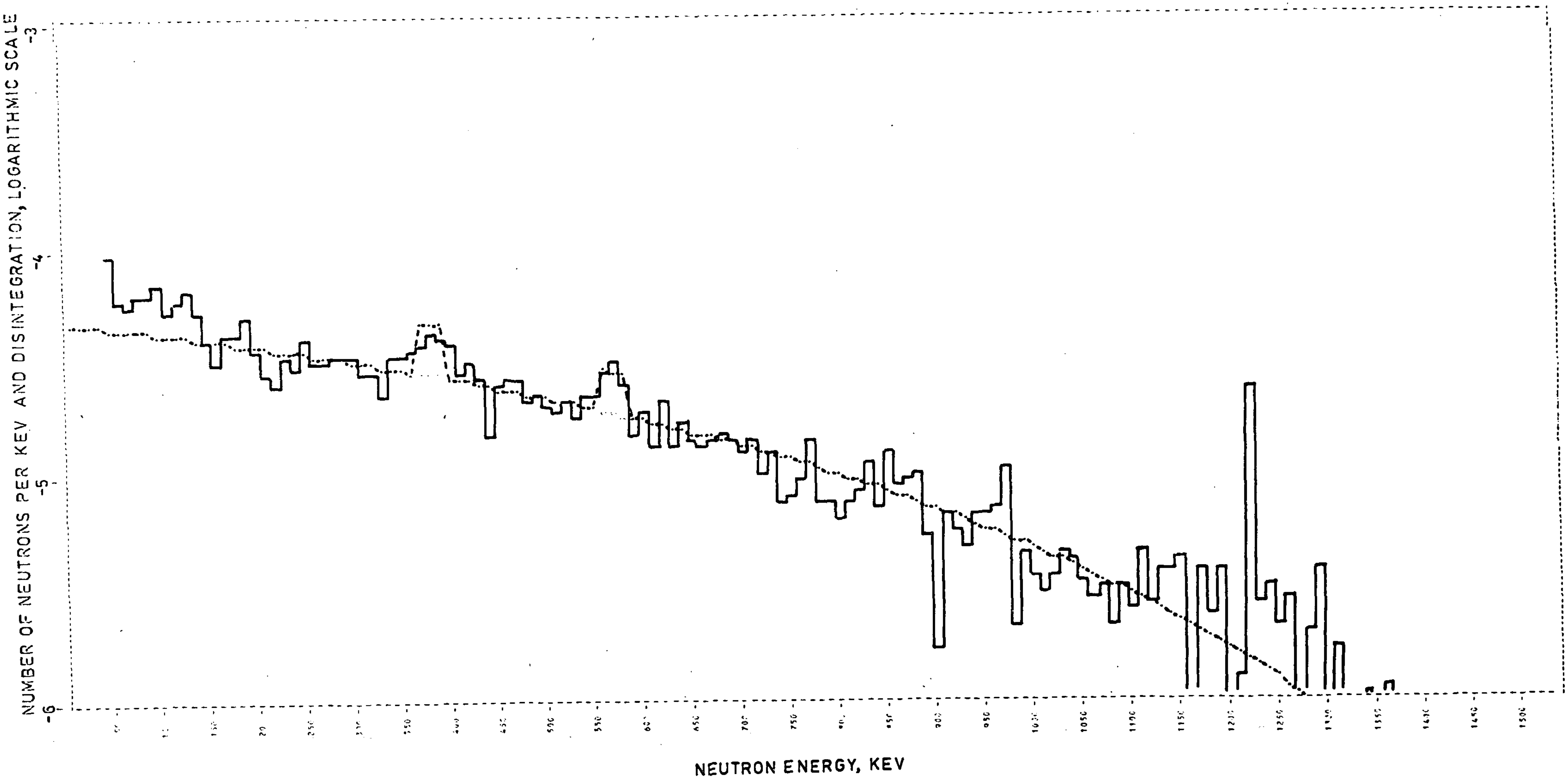

Fig. 19. Experimental and calculated delayed-neutron spectra for the precursor ^{138}I
Histogram: Experimental spectrum[4)]
Dotted curve: Calculated spectrum
Curve denoted by S: s-wave component

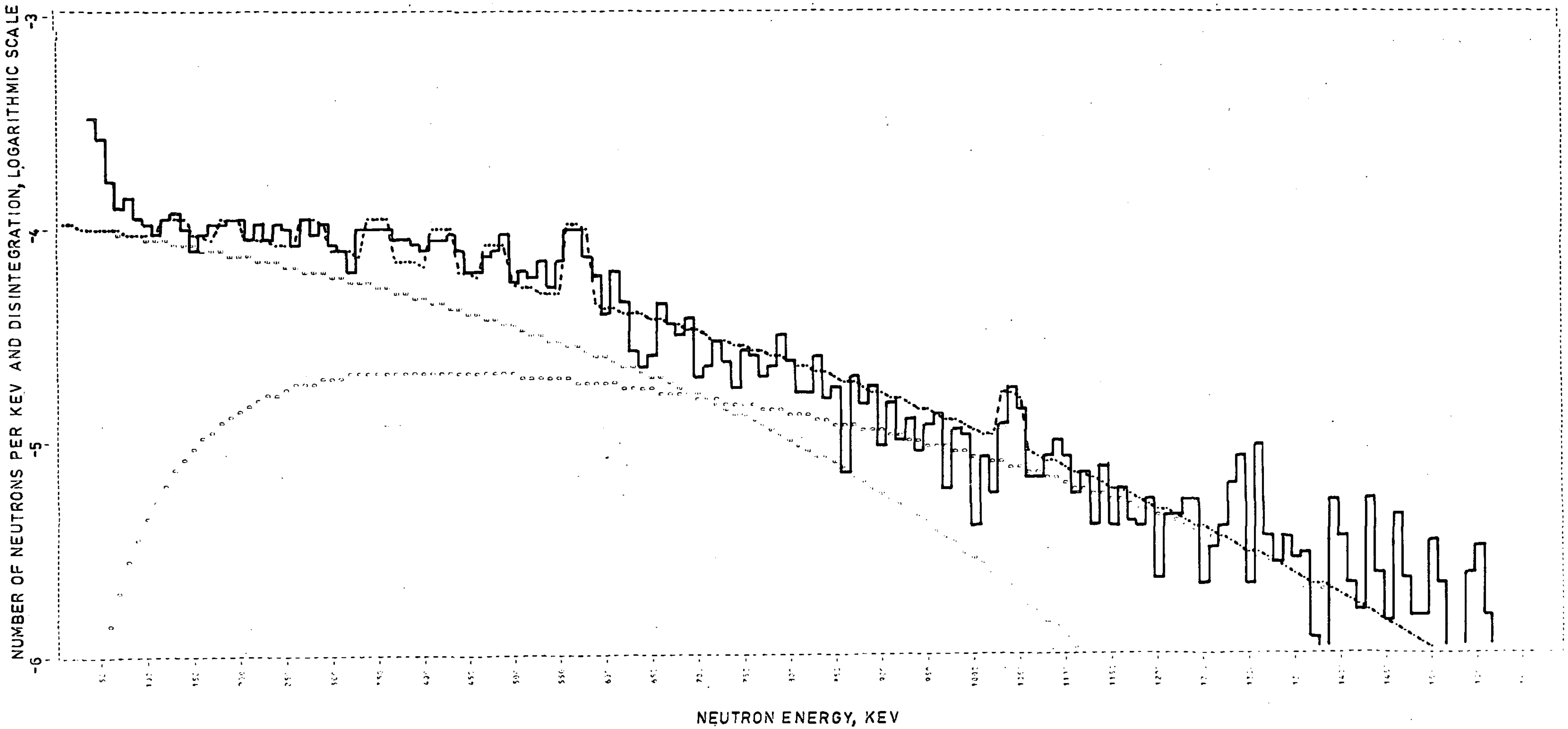

Fig. 20. Experimental and calculated delayed-neutron spectra for the precursor ^{139}I
Histogram: Experimental spectrum[3)]
Dotted curve: Calculated spectrum
Curve denoted by E: s-wave component to the level at 593 keV in ^{138}Xe
Curve denoted by D: d-wave component

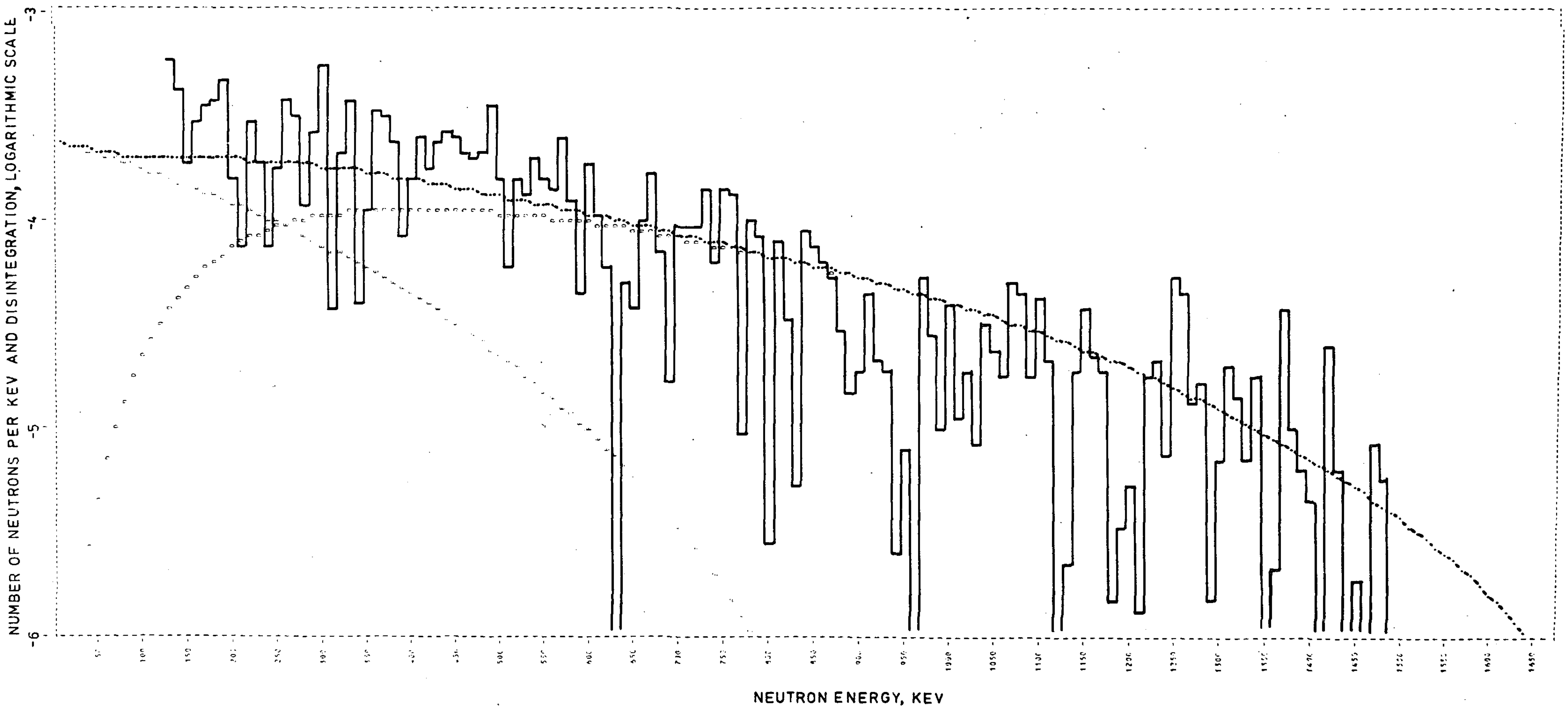

Fig. 21. Experimental and calculated delayed-neutron spectra for the precursor ^{140}I
Histogram: Experimental spectrum[4)]
Dotted curve: Calculated spectrum
Curve denoted by E: s-wave component to a hypothetical level at 1.0 MeV in ^{139}Xe
Curve denoted by D: d-wave component

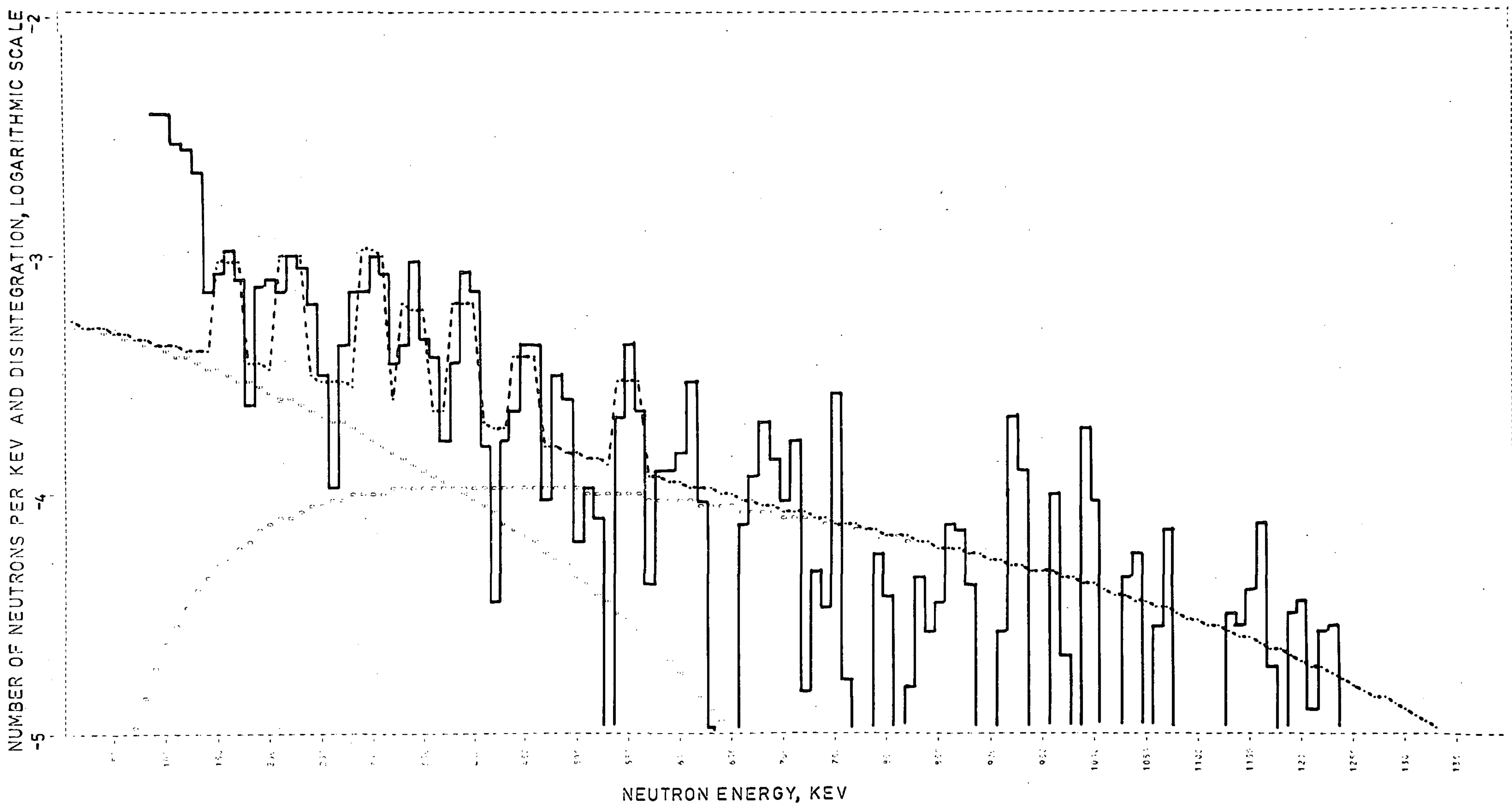

Fig. 22. Experimental and calculated delayed-neutron spectra for the precursor ^{141}I
Histogram: Experimental spectrum[3)]
Dotted curve: Calculated spectrum
Curve denoted by E: s-wave component to a hypothetical level at 1.0 MeV in ^{140}Xe
Curve denoted by D: d-wave component

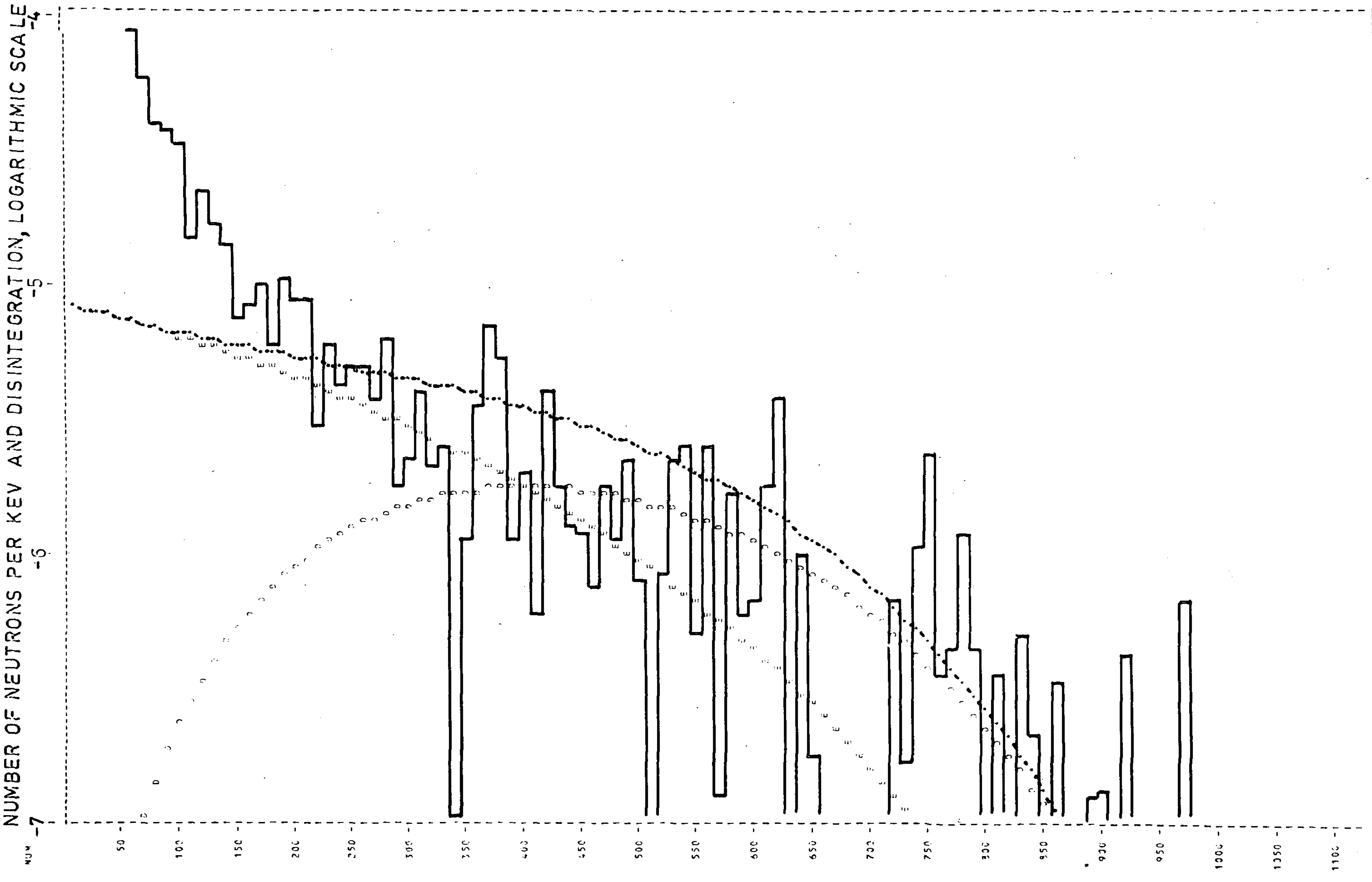

Fig. 23. Experimental and calculated delayed-neutron spectra for the precursor ^{142}Cs
Histogram: Experimental spectrum[4)]
Dotted curve: Calculated spectrum
Curve denoted by E: s-wave component to the level at 490 keV in ^{141}Ba
Curve denoted by D: d-wave component

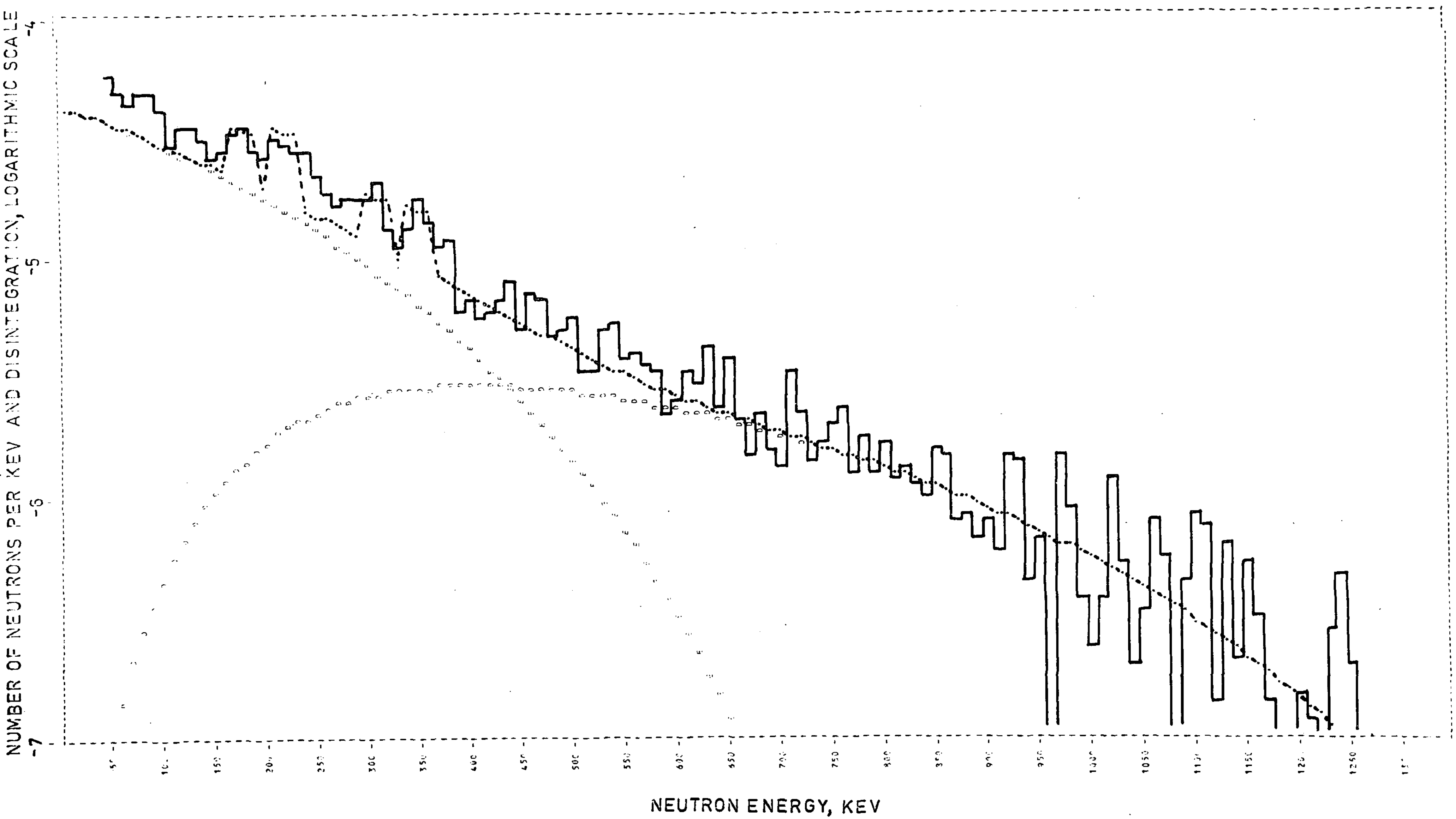

Fig. 24. Experimental and calculated delayed-neutron spectra for the precursor ^{143}Cs
Histogram: Experimental spectrum[3)]
Dotted curve: Calculated spectrum
Curve denoted by E: s-wave component to the level at 835 keV in ^{142}Ba
Curve denoted by D: d-wave component

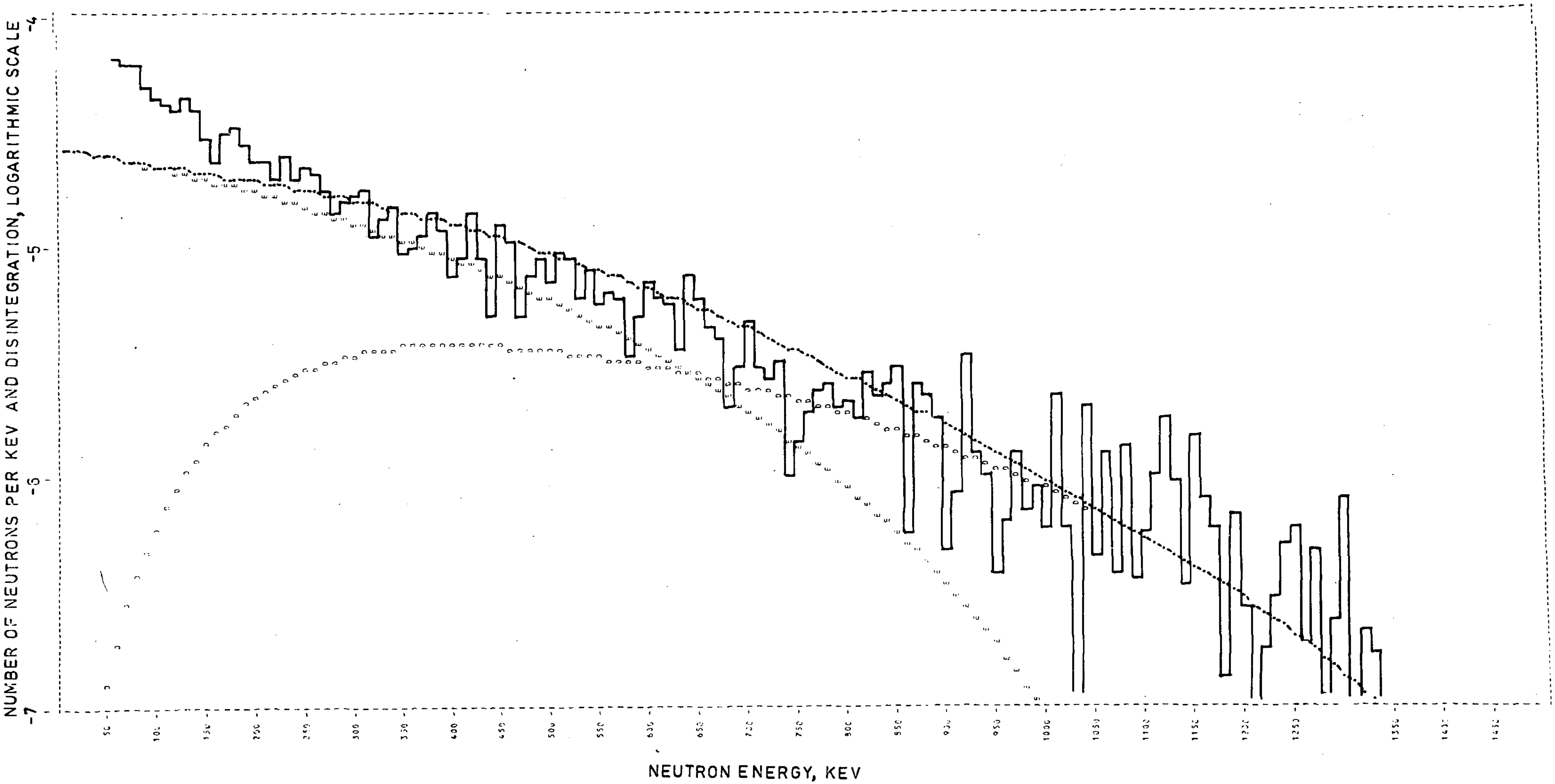

Fig. 25. Experimental and calculated delayed-neutron spectra for the precursor ^{144}Cs
Histogram: Experimental spectrum[4)]
Dotted curve: Calculated spectrum
Curve denoted by E: s-wave component to a hypothetical level at 0.5 MeV in ^{143}Ba
Curve denoted by D: d-wave component

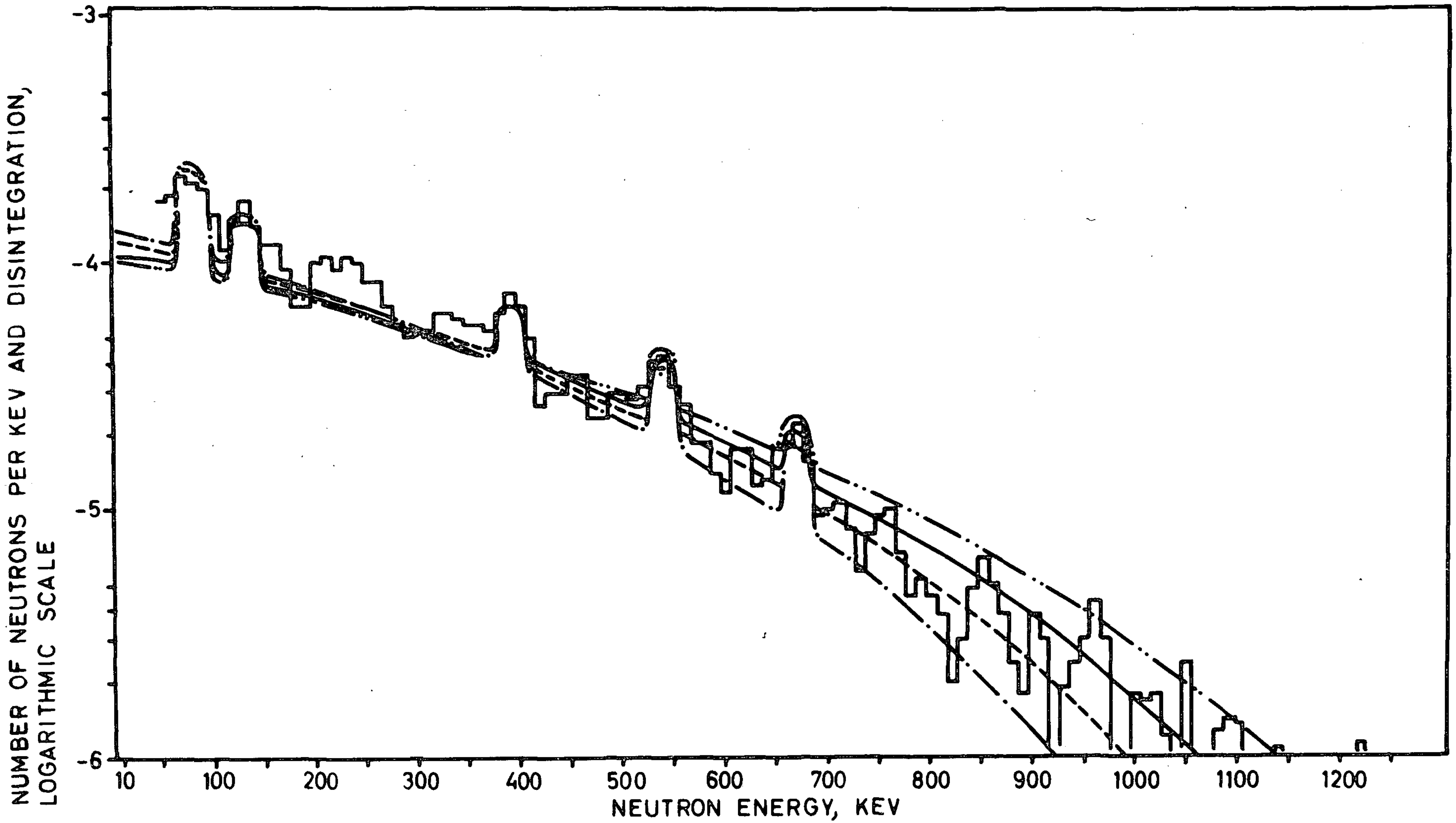

Fig. 26. Experimental and calculated delayed-neutron spectra for the precursor ^{88}Br.
Histogram: Experimental spectrum[4)]
Dash-dot curve: Q_β = 8.4 MeV
Dashed curve: Q_β = 8.5 MeV
Solid curve: Q_β = 8.6 MeV
Dash-dot-dot curve: Q_β = 8.7 MeV

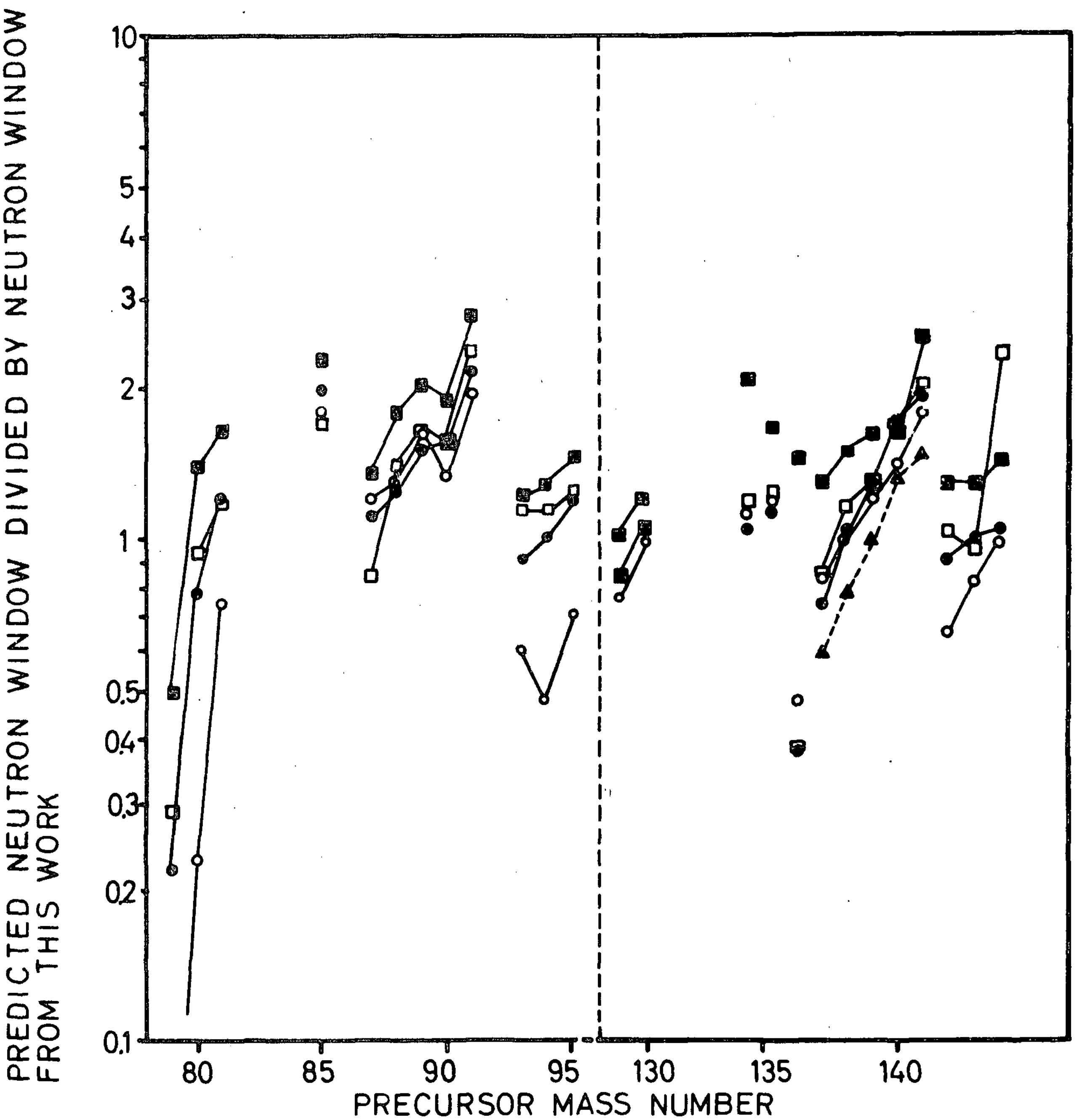

Fig. 27. Ratio between predicted neutron windows and windows deduced in the present work.
Closed circles: Values predicted from ref.[17)]
Open circles: Values predicted from ref.[18)]
Closed squares: Values predicted from ref.[19)]
Open squares: Values predicted from ref.[20)]
Closed triangles: Values predicted from ref.[17)] with windows deduced assuming a constant beta-strength.
Isotopic chains have been joined by solid lines (first four cases) or by a dashed line (last case).

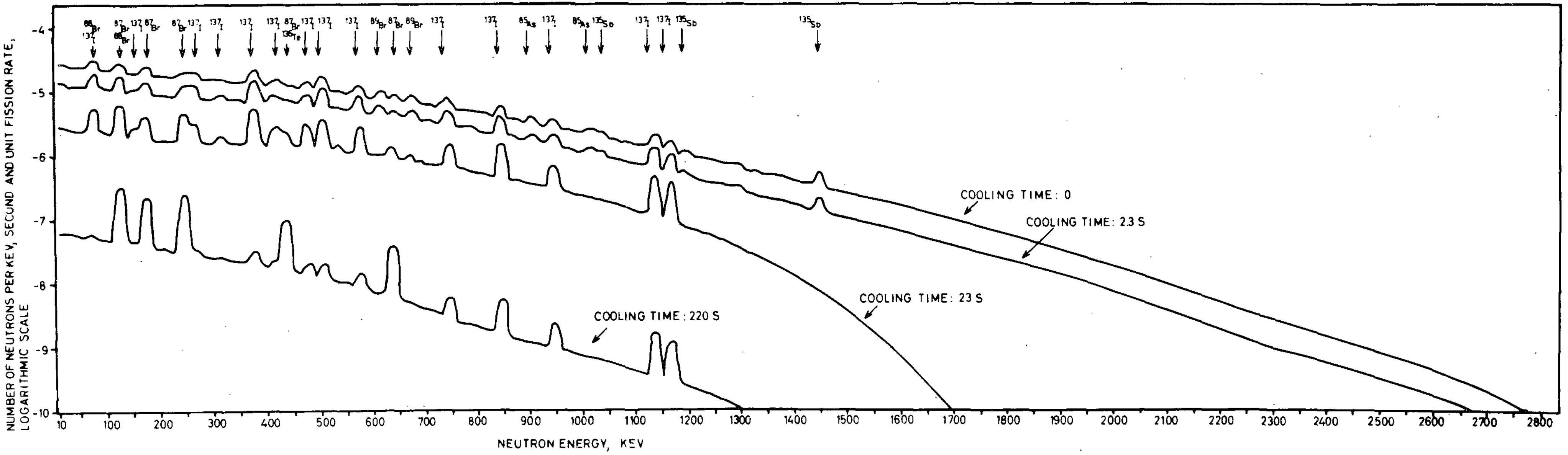

Fig. 28. Delayed-neutron spectra for a long irradiation of ^{235}U and cooling times 0, 2.3 s, 23 s, and 220 s. The origin of the fine structure peaks is indicated. In the other figures of the present article the peaks have been spread out over 30 keV, but in this figure 20 keV has been used instead to make the peaks more clearly visible.

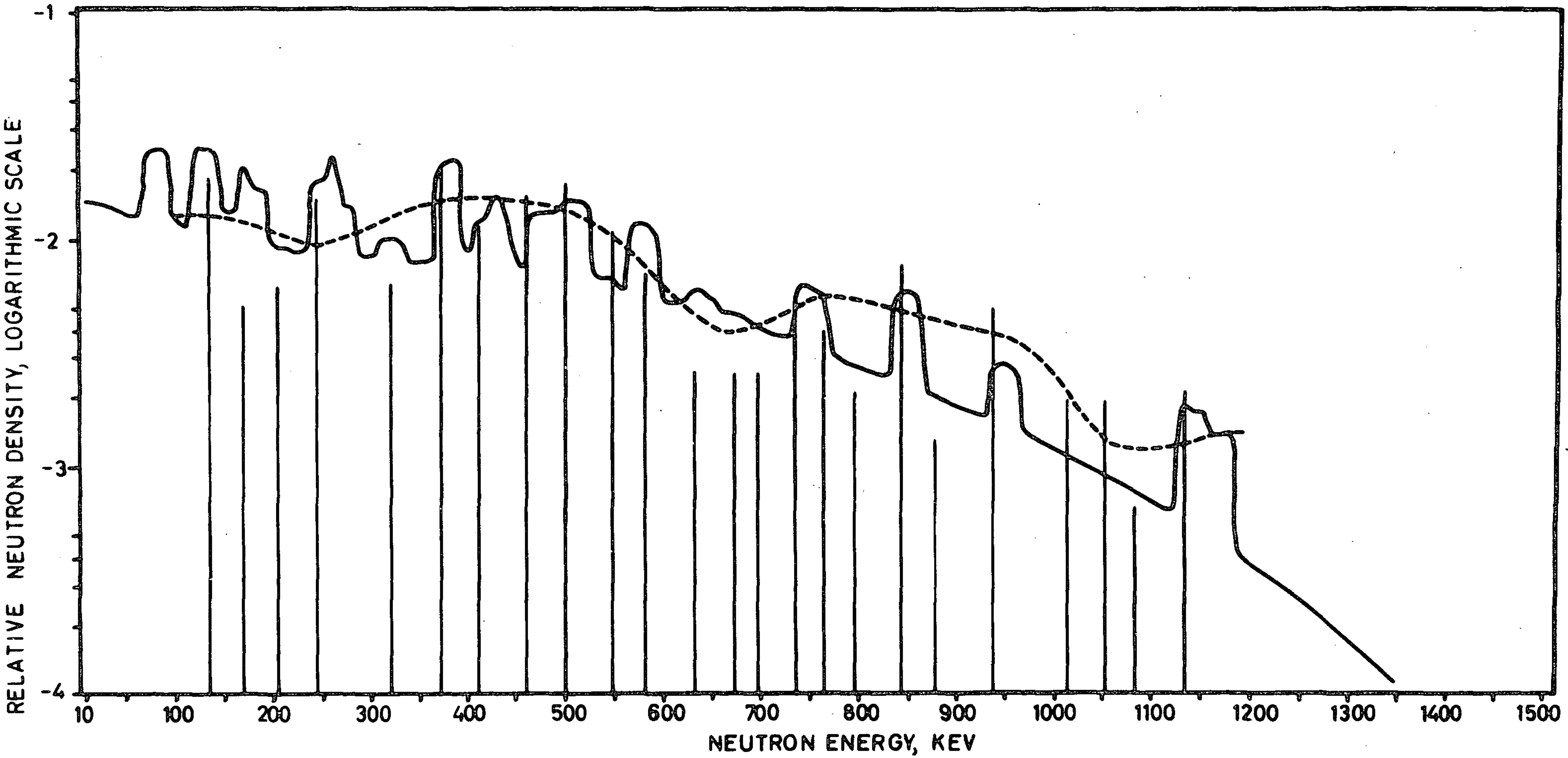

Fig. 29. Experimental and calculated effective delayed-neutron spectra in the fission of ^{235}U.
Experimental conditions: T = 60 s; t_c = 18 s; t_m = 48 s; t_{tot} = 178 s
Staples: Experimental peaks from ref. 41)
Dashed curve: Experimental spectrum (smoothed)
Solid curve: Calculated spectrum

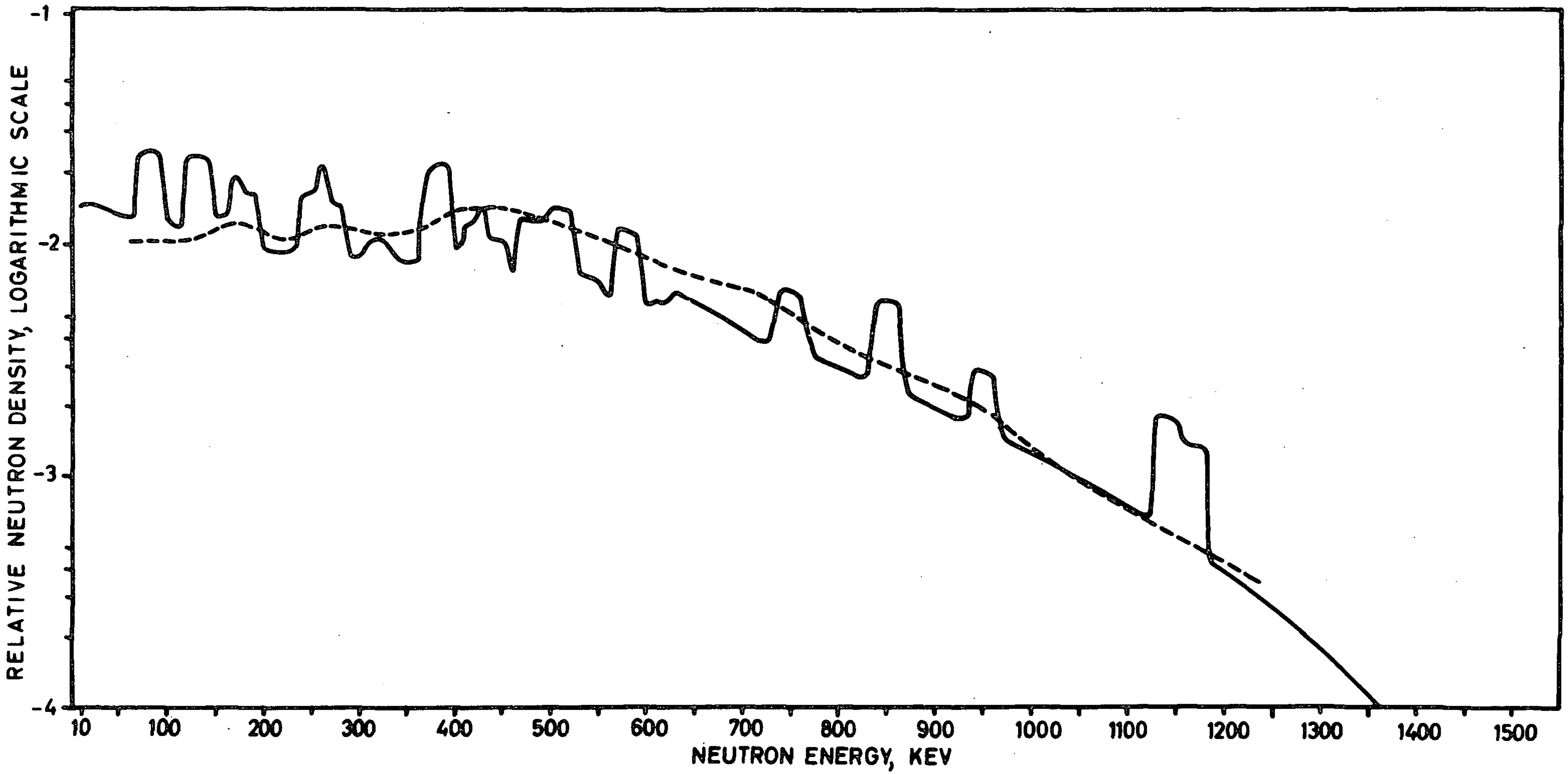

Fig. 30. Experimental and calculated effective delayed-neutron spectra in the fission of ^{235}U.
Experimental conditions: $T = 115$ s; $t_c = 10$ s; $t_m = 28$ s; $t_{tot} = 240$ s.
Dashed curve: Experimental spectrum from ref.[42)]
Solid curve: Calculated spectrum

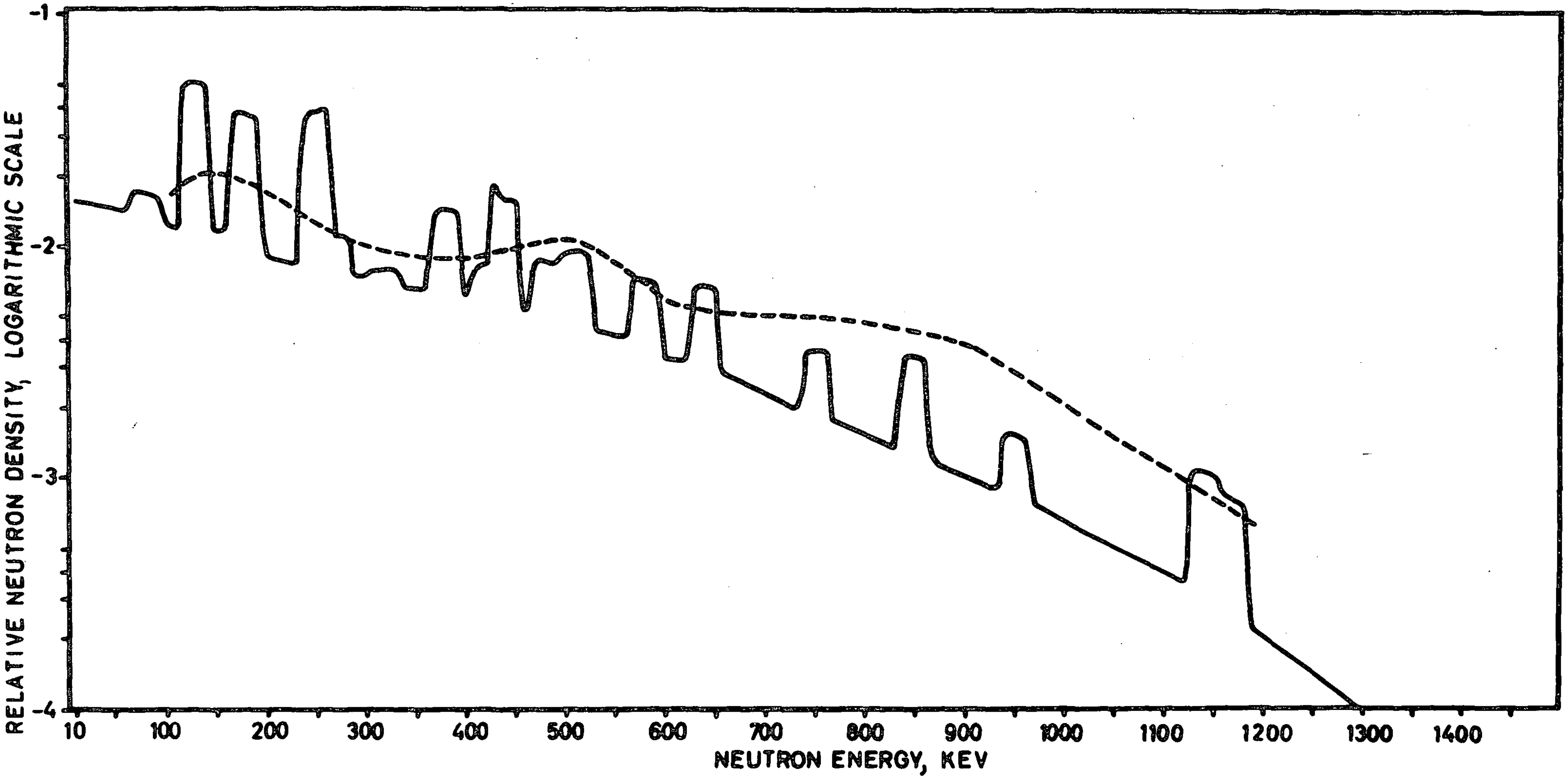

Fig. 31. Experimental and calculated effective delayed-neutron spectra in the fission of ^{235}U.
Experimental conditions: $T = 150$ s; $t_c = 100$ s; $t_m = 100$ s; $t_{tot} = 360$ s.
Dashed curve: Experimental spectrum from ref.[42)]
Solid curve: Calculated spectrum

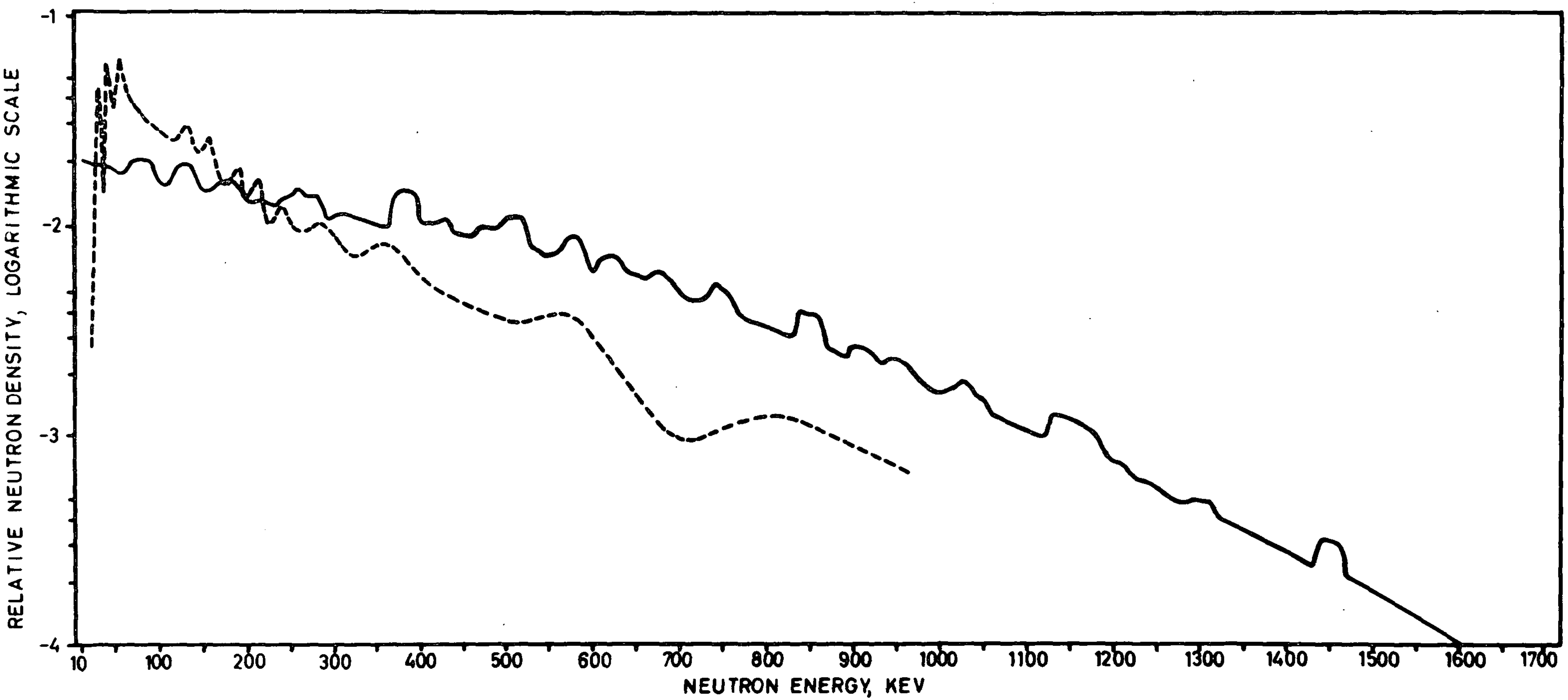

Fig. 32. Experimental and calculated effective delayed-neutron spectra in the fission of ^{235}U.
Experimental conditions: $T = 1.9$ s; $t_c = 0.2$ s; $t_m = 1.8$ s; $t_{tot} = 4.0$ s.
Dashed curve: Experimental spectrum from ref.[43])
Solid curve: Calculated spectrum

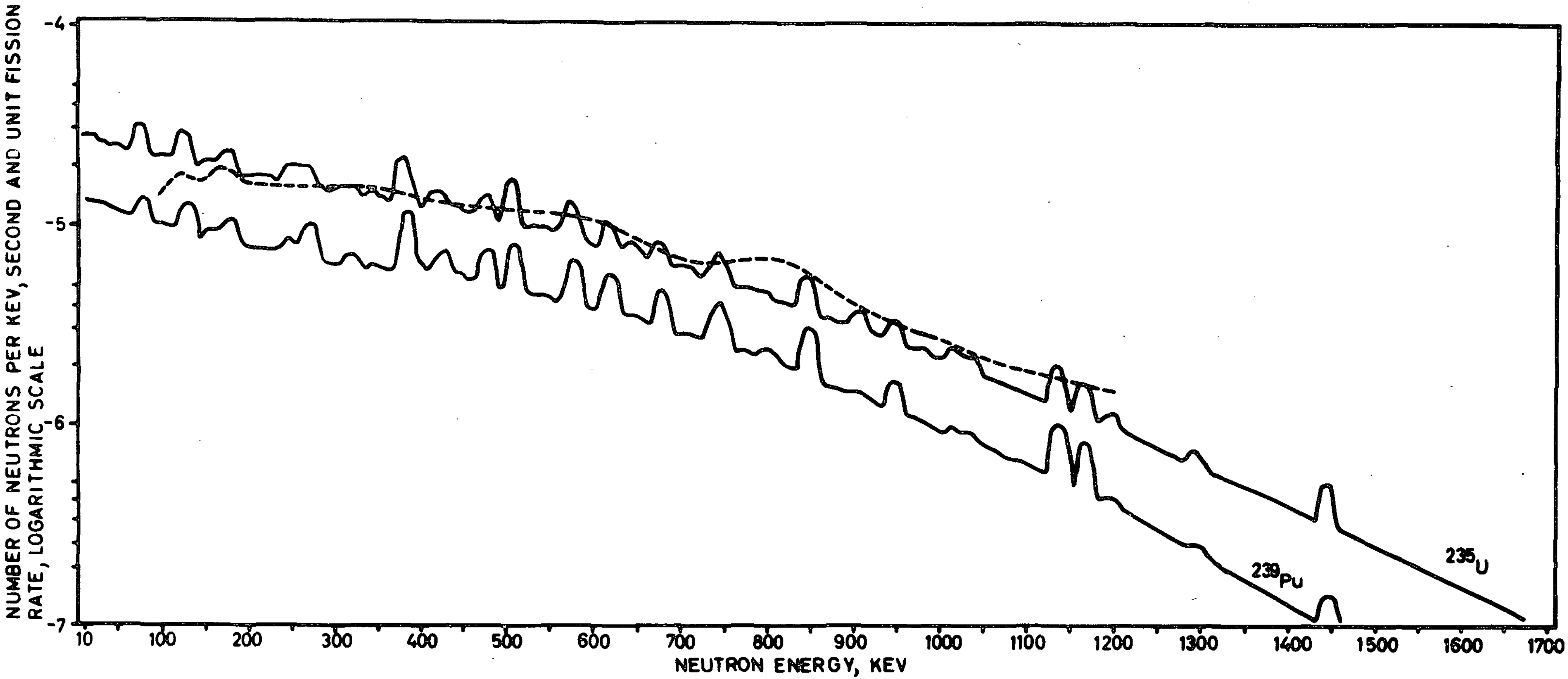

Fig. 33. Equilibrium spectra of delayed neutrons.

Upper solid curve: Calculated spectrum for ^{235}U

Lower solid curve: Calculated spectrum for ^{239}Pu

Dashed curve: Spectrum for ^{235}U deduced by Fieg[42)]